2004-10-01

Phosphatidylinositol-4,5-bisphosphate-rich plasma membrane patches organize active zones of endocytosis and ruffling in cultured adipocytes

Shaohui Huang
University of Massachusetts Medical School

Et al.

MOLECULAR AND CELLULAR BIOLOGY, Oct. 2004, p. 9102–9123 Vol. 24, No. 20
0270-7306/04/$08.00+0 DOI: 10.1128/MCB.24.20.9102–9123.2004

Phosphatidylinositol-4,5-Bisphosphate-Rich Plasma Membrane Patches Organize Active Zones of Endocytosis and Ruffling in Cultured Adipocytes

Shaohui Huang,[1] Larry Lifshitz,[2] Varsha Patki-Kamath,[1] Richard Tuft,[2] Kevin Fogarty,[2] and Michael P. Czech[1]*

Program in Molecular Medicine[1] and Biomedical Imaging Group, Department of Physiology,[2] University of Massachusetts Medical School, Worcester, Massachusetts

Received 22 December 2003/Returned for modification 1 March 2004/Accepted 2 July 2004

A major regulator of endocytosis and cortical F-actin is thought to be phosphatidylinositol-4,5-bisphosphate [PtdIns(4,5)P_2] present in plasma membranes. Here we report that in 3T3-L1 adipocytes, clathrin-coated membrane retrieval and dense concentrations of polymerized actin occur in restricted zones of high endocytic activity. Ultrafast-acquisition and superresolution deconvolution microscopy of cultured adipocytes expressing an enhanced green fluorescent protein- or enhanced cyan fluorescent protein (ECFP)-tagged phospholipase Cδ1 (PLCδ1) pleckstrin homology (PH) domain reveals that these zones spatially coincide with large-scale PtdIns(4,5)P_2-rich plasma membrane patches (PRMPs). PRMPs exhibit lateral dimensions exceeding several micrometers, are relatively stationary, and display extensive local membrane folding that concentrates PtdIns(4,5)P_2 in three-dimensional space. In addition, a higher concentration of PtdIns(4,5)P_2 in the membranes of PRMPs than in other regions of the plasma membrane can be detected by quantitative fluorescence microscopy. Vesicular structures containing both clathrin heavy chains and PtdIns(4,5)P_2 are revealed immediately beneath PRMPs, as is dense F actin. Blockade of PtdIns(4,5)P_2 function in PRMPs by high expression of the ECFP-tagged PLCδ1 PH domain inhibits transferrin endocytosis and reduces the abundance of cortical F-actin. Membrane ruffles induced by the expression of unconventional myosin 1c were also found to localize at PRMPs. These results are consistent with the hypothesis that PRMPs organize active PtdIns(4,5)P_2 signaling zones in the adipocyte plasma membrane that in turn control regulators of endocytosis, actin dynamics, and membrane ruffling.

Phosphatidylinositol-4,5-bisphosphate [PtdIns(4,5)P_2] constitutes only about 1% of the total phospholipid in the plasma membrane but plays major roles in regulating multiple cellular processes. Classically, PtdIns(4,5)P_2 was established as the precursor of two intracellular second messengers, inositol-1,4,5-trisphosphate [Ins(3,4,5)P_3] and diacylglycerol, generated through the regulation of phospholipase C (PLC) (57). The subsequent discovery of phosphoinositide 3-kinases (9) revealed that PtdIns(4,5)P_2 was also the substrate for the synthesis of phosphatidylinositol-3,4,5-trisphosphate [PtdIns(3,4,5)P_3], an important second messenger involved in insulin and growth factor signaling, cytoskeletal remodeling, and cell proliferation and survival (63, 65). More recently, it was shown that PtdIns(4,5)P_2 itself functions to regulate the actin cytoskeleton, membrane trafficking, and plasma membrane ion channels and transporters (14, 15, 24, 25, 54, 58, 62). Consequently, this extraordinary versatility of PtdIns(4,5)P_2 in cellular signaling led to the suggestion that there are spatially and functionally segregated pools of PtdIns(4,5)P_2 in the plasma membrane (32, 43, 44, 48). Furthermore, unlike conventional signaling molecules [e.g., Ca^{2+}, Ins(3,4,5)P_3, and PtdIns(3,4,5)P_3] that, upon receptor activation, show dramatic increases in concentrations from very low levels, the overall PtdIns(4,5)P_2 concentration in the plasma membrane is already quite high in unstimulated cells and is unlikely to increase further upon antagonist stimulation (44, 48, 62). Thus, the hypothesis that PtdIns(4,5)P_2 itself is a second messenger depends upon whether its concentration is locally regulated in response to cell stimulation without a marked change in its overall plasma membrane concentration (44, 58, 62).

Biochemical studies initially suggested that PtdIns(4,5)P_2 might be enriched in caveolin-rich detergent-insoluble membrane rafts (DIMRs) (28, 69). Later studies contradicted this early result but supported the hypothesis that PtdIns(4,5)P_2 instead might be concentrated in caveolin-free DIMRs (68, 70). However, the polyunsaturated lipid tails of PtdIns(4,5)P_2 make the polyphosphoinositide unsuitable for spontaneous partitioning into DIMRs (41). Recently, proteins in the GMC family, which includes the neuronal proteins GAP43, myristoylated alanine-rich C kinase substrate (MARCKS), and CAP23, were found to promote PtdIns(4,5)P_2 clustering in presumed membrane rafts in neuronal cells (38). MARCKS was further proposed to reversibly sequester plasma membrane PtdIns(4,5)P_2 and to regulate its availability in response to extracellular stimuli (1, 44). This hypothesis is proposed to account for the fact that PtdIns(4,5)P_2 is also apparently enriched in large-scale (i.e., micrometer-sized) plasma membrane structures, such as lamellipodia (68), membrane ruffles (27), and contact sites for bacterial invasion (60) and phagocytosis (6).

PtdIns(4,5)P_2 has also been shown to promote actin polymerization at sites where membrane retrieval and insertion are

* Corresponding author. Mailing address: Program in Molecular Medicine, University of Massachusetts Medical School, 373 Plantation St., Worcester, MA 01605. Phone: (508) 856-2254. Fax: (508) 856-1617. E-mail: Michael.Czech@umassmed.edu.

active, and a hypothetical signaling mechanism has emerged to account for this activity. According to this concept, localized PtdIns(4,5)P_2 concentrations result from the recruitment of phosphatidylinositol 4-phosphate 5-kinase α to specialized regions of the plasma membrane in response to activation of the small G proteins Rac-1 and ARF6 (6, 16, 26, 27). However, this view was recently challenged based on biophysical characterizations of PtdIns(4,5)P_2 in cell membranes (66). These new data suggest that apparent localized increases in plasma membrane PtdIns(4,5)P_2 concentrations simply reflect increased amounts of total membrane constituents in these regions. Such membrane-rich domains are apparently caused by local membrane folds that are not resolved by fluorescence microscopy (13, 46, 66). Furthermore, measurements of fluorescence recovery after photobleaching suggest that lipid diffusion in the lipid bilayer is too fast to maintain these apparently PtdIns(4,5)P_2-rich membrane regions (13, 42, 66). Taken together, the available data provide a confusing representation of the organization and dynamics of PtdIns(4,5)P_2 in the plasma membrane and the exact role of PtdIns(4,5)P_2 in regulating cellular processes.

The present studies were designed to clarify the disposition and dynamics of the endocytosis regulator PtdIns(4,5)P_2 in insulin-sensitive adipocytes in three-dimensional (3D) space by using ultrafast-acquisition and superresolution deconvolution microscopy (11, 51). We focused these studies on visualizing a green fluorescent protein (GFP)-tagged probe for PtdIns(4,5)P_2 in cultured 3T3-L1 adipocytes, which display active membrane trafficking, a large surface area, and a significant vertical dimension. The novel approach developed here revealed surprisingly large-scale PtdIns(4,5)P_2-rich plasma membrane patches (PRMPs) with lateral dimensions exceeding several micrometers and sometimes extending from the bottom to the top of a cell. Control experiments with membrane-staining reagents revealed that local membrane folds were responsible for these PtdIns(4,5)P_2-rich structures but also revealed a higher lateral PtdIns(4,5)P_2 concentration in the lipid bilayer. PRMPs associate exclusively with regions of dense F actin and colocalize with highly active zones of massive endocytosis heterogeneously displayed on the cell surface. Endocytosis of transferrin and cortical F-actin formation indeed require functional PtdIns(4,5)P_2. Remarkably, PRMPs also appear to define active regions of membrane ruffling induced by the expression of unconventional myosin 1c (Myo1c). Taken together, the data define a novel plasma membrane domain in cultured adipocytes that concentrates PtdIns(4,5)P_2 in 3D space to apparently regulate important plasma membrane functions.

MATERIALS AND METHODS

DNA constructs. Previously characterized plasmid constructs (pEGFP-N1; Clontech, Palo Alto, Calif.) containing the pleckstrin homology (PH) domain of PLCδ1 linked to enhanced GFP (EGFP) (EGFP/PLCδ1-PH) or a PtdIns(4,5)P_2-binding-deficient mutant (R40L) were generous gifts from Tamás Balla (National Institutes of Health, Bethesda, Md.). The inserts of the PLCδ1 PH domain and the corresponding mutant were amplified by PCR with primers 5′-TCAAG CTTCGAATTAACGGCATGGACT-3′ and 5′-TGGATCCTTTCTAGAGTTC TGCAGCTA-3′. Following digestion with EcoRI and XbaI, the purified PCR products were ligated to the same multiple cloning sites in plasmid pECFP-C1 (Clontech). The correct inserts were verified by sequencing. Plasmid pEYFP-C1 (Clontech) containing Myo1c was previously characterized (4). The pcDNA3.1 construct containing the human transferrin receptor (hTFRc) was a generous gift from Haley Melikian (University of Massachusetts Medical School).

Cell culture and fluorescent labeling of the plasma membrane. 3T3-L1 fibroblasts (American Type Culture Collection, Manassas, Va.) were grown to confluence and differentiated as described previously (47). Day 6 to day 8 differentiated adipocytes were electroporated (47) with 50 μg of EGFP/PLCδ1-PH, ECFP/PLCδ1-PH (enhanced cyan fluorescent protein [ECFP] linked to the PH domain of PLCδ1) or EYFP/Myo1c (enhanced yellow fluorescent protein [EYFP] linked to Myo1c) plasmid DNA and subsequently plated on no. 1.5 coverslips (Thomas Scientific, Swedesboro, N.J.). Transfected cells were grown in Dulbecco's modified Eagle's medium (DMEM) with 10% fetal calf serum (complete DMEM) for >12 h before being switched to DMEM without fetal calf serum (serum-starved medium). Penicillin at 50 U/ml and streptomycin at 50 μg/ml were always included to prevent bacterial contamination.

After >2 h of serum starvation, live-cell microscopy was carried out at 37°C with KRH buffer (125 mM NaCl, 5 mM KCl, 1.3 mM $CaCl_2$, 1.2 mM $MgSO_4$, 2 mM sodium pyruvate, 25 mM HEPES [pH 7.4], 0.2% [wt/vol] bovine serum albumin). Insulin stimulation of serum-starved cells was carried out at 37°C with 100 nM human insulin (Eli Lilly, Indianapolis, Ind.). Alternatively, cells were fixed in 4% (wt/vol) formaldehyde at room temperature for 12 min and preserved in ProLong immersion medium for superresolution deconvolution microscopic studies. Following permeabilization of fixed cells with 0.5% (vol/vol) Triton X-100, F-actin was stained with rhodamine (RhD)-conjugated phalloidin (RhD-PhD). Alternatively, endogenous clathrin heavy chains were targeted with a rabbit polyclonal antibody developed in the laboratory of Silvia Corvera (University of Massachusetts Medical School), followed by immunofluorescence staining with an RhD-conjugated goat anti-rabbit secondary antibody. Depending on the experiment, plasma membrane staining with ~5 μg of Alexa488 (Alx488)- or Alexa594 (Alx594)-conjugated concanavalin A (ConA)/ml for 2 to 5 min, ~1 μM BODIPY-HPC for ~30 min, or ~1 μM DiIC18 for ~5 min was carried out with live or fixed adipocytes and at 4°C (to inhibit endocytosis), room temperature (for fixed cells), or 37°C (for live cells). All fluorescent reagents and ProLong immersion medium were purchased from Molecular Probes (Eugene, Oreg.).

Transferrin endocytosis. Day 4 differentiated 3T3-L1 adipocytes were coelectroporated with 50 and 150 μg of plasmid DNAs containing hTFRc and EGFP/PLCδ1-PH sequences, respectively. The cells were cultured overnight at 37°C. The adipocytes were washed once with KRH buffer, cooled to 4°C, and incubated at 4°C for 1 h in KRH buffer with 20 μg of Alx488-conjugated transferrin (Alx488-TF; Molecular Probes)/ml. Subsequently, the cells were warmed to 37°C and incubated for 15 min to allow Alx488-TF uptake. Another set of adipocytes was electroporated with 50 μg of hTFRc DNA alone and treated with 60 μM latrunculin B (LB) for 2 h at 37°C before Alx488-TF labeling and uptake experiments were carried out. The cells were washed three times with ice-cold phosphate-buffered saline and immediately fixed in 4% formaldehyde. Fixed cells were labeled with RhD-PhD for F-actin.

Microscopy. The laser-illuminated ultrafast-acquisition microscope and its applications to investigations of cellular dynamics have been described in detail elsewhere (47, 51). Coupled with a Nikon 60× 1.40-numerical-aperture (NA) oil objective, the setup was able to acquire image stacks with a low pixel resolution of 333 nm and *z* spacing of 250 nm. This spatial combination produced ripple-like patterns in the deconvolved images (see Fig. 1, 2, and 13) that should be regarded as continuous regions. High-magnification imaging (see Fig. 5, 7 to 9, and 12) with a pixel size of 66 nm and *z* spacing of 250 nm was carried out by using a Zeiss Axiovert 200 M microscope equipped with a 100× 1.40-NA oil objective. Image stacks were deconvolved with the superresolution deconvolution algorithm developed by Carrington et al. (11). On the high-magnification images, the above-mentioned ripple-like patterns are almost not noticeable.

Image rendering and analysis were carried out using Data Analysis and Visualization Environment (40) and other software tools developed by the Biomedical Imaging Group at the University of Massachusetts Medical School (http://invitro.umassmed.edu). Typically, the dynamic range (i.e., the minimum to maximum pixel intensity ranges) of 12- and 14-bit images obtained from the ultrafast-acquisition and Zeiss microscopes, respectively, was first linearly mapped to the full scale (i.e., 0 to 255) of an 8-bit gray or false-color intensity scale. The images were further rescaled to a narrower intensity range (i.e., contrast enhanced). The deformable snake algorithm (71) was modified slightly for use with our data and was used to automatically find cell boundaries (see Fig. 3 and 4). With the aid of the Align program (http://invitro.umassmed.edu), images of the same cell obtained with different fluorescence channels were visually aligned to within ~1 pixel of each other.

Filter sets were purchased from Chroma Techology Co. (Battleboro, Vt.) for imaging ECFP (i.e., CFP channel; filter set 31044 v2), EGFP-Alx488 (i.e., GFP

channel; 41001), Alx488-ConA/Alx488-TF (i.e., YFP channel; 41028), and Alx594-ConA/RhD (i.e., RhD channel; CZ914) fluorescence. Cross talk among fluorescence channels was characterized with specimens from single-fluorophore labeling and was found to be negligible. Occasionally, Alx488-ConA/Alx488-TF fluorescence was deliberately imaged in the YFP channel in three-color colocalization studies (see Fig. 5, 9, and 10) to avoid fluorescence bleedthrough from the CFP channel.

Quantitative image analysis. A fluorescence image (F) can be approximated as the convolved product of the fluorescent specimen [$S(r)$], the point spread function (PSF), and the spatial detection efficiency function [$D(r')$] of the microscope, so that $F = \int\int D(r') \times S(r) \times \mathrm{PSF} \times dr \times dr'$. For the green ($F_G$) and red ($F_R$) fluorescence images of the same specimen, $\Delta F = F_G - F_R = [\int\int D(r')_G \times S(r)_G \times \mathrm{PSF}_G \times dr \times dr'] - [\int\int D(r')_R \times S(r)_R \times \mathrm{PSF}_R \times dr \times dr']$. In this study, the green image is associated with the EGFP/PLCδ1-PH label, and the red one is associated with the BODIPY-HPC/Alx594-ConA probe (see Fig. 3 and 4). $D(r')$ is a property of the microscope system, and when F_G and F_R are appropriately normalized (see Results), $D(r')_G \approx D(r')_R$. The measured PSFs are very similar (i.e., $\mathrm{PSF}_G \approx \mathrm{PSF}_R$), consistent with the negligible chromatic effect observed in the deconvolved images. Consequently, $\Delta F \approx \int\int D(r') \times \mathrm{PSF} \times [S(r)_G - S(r)_R] \times dr \times dr'$. Thus, ΔF reflects only the difference in the fluorescent probes present in the specimens, as it should. This scenario was confirmed in a control experiment, in which ratiometric analysis of an EGFP/PLCδ1-PH fluorescence image and its counterpart detected in the YFP channel by use of bleedthrough signals revealed that little systematic error was introduced by the microscope system (see Fig. S1 at http://invitro.umassmed.edu/~sh/supplements/supplements.html).

RESULTS

PtdIns(4,5)P_2 is concentrated in PRMPs in live 3T3-L1 adipocytes. In this study, we used an ultrafast-acquisition deconvolution microscope to image the real-time distribution of PtdIns(4,5)P_2 in live 3T3-L1 adipocytes. PtdIns(4,5)P_2 was visualized by transient expression of a fusion protein linking EGFP to the PH domain of PLCδ1 (EGFP/PLCδ1-PH) (Fig. 1) (3). With this technique, a typical 3D image consisting of 81 z sections (~20 μm thick) (Fig. 1A or C) can be acquired in about 1 s. Because of the high efficiency of utilizing fluorescence photons and thus the relatively low excitation power used, the ultrafast-acquisition deconvolution microscope is least affected by photobleaching. With wide-field illumination, it is also the fastest way to acquire 3D images. These characteristics proved to be important for capturing real-time fluorescence images that closely represent the distribution and dynamics of PtdIns(4,5)P_2 in live cells.

PtdIns(4,5)P_2 is primarily localized to the plasma membrane of cultured adipocytes (Fig. 1), consistent with previous observations obtained when EGFP/PLCδ1-PH was used as the fluorescent marker in other cell lines (6, 56, 66, 67). In contrast, the EGFP/PLCδ1-PH mutant deficient in PtdIns(4,5)P_2 binding (i.e., R40L) (67) shows no plasma membrane localization but a mostly uniform fluorescence distribution in the cytoplasm of 3T3-L1 adipocytes (see Fig. S2 at http://invitro.umassmed.edu/~sh/supplements/supplements.html). Surprisingly, we found that PtdIns(4,5)P_2 is enriched in distinct regions at the adipocyte surface (Fig. 1; see also movie 1 at http://invitro.umassmed.edu/~sh/supplements/supplements.html). Large-scale PtdIns(4,5)P_2-rich membrane domains (red regions in Fig. 1A, C, and D) with lateral dimensions exceeding several micrometers are observed and sometimes extend through almost the entire height of the cell (Fig. 1A). These PtdIns(4,5)P_2-rich domains are found in both serum-starved cells (Fig. 1A and D) and insulin-stimulated cells (Fig. 1C). The fact that most of these domains are organized perpendicular to the coverslip-attached plasma membrane suggests that they are not artifacts of photobleaching during image acquisition. These domains are visualized with 8-bit, contrast-enhanced, false-color intensity scales (intensity scale bar in Fig. 1A; see Materials and Methods) and are the approximation of their counterparts shown in the corresponding 8-bit gray-scale image without contrast enhancement (inset in Fig. 1A). Within these domains, gradients of PtdIns(4,5)P_2 distribution also exist, as exemplified by the 2D intensity plot (Fig. 1B; see also movie 1 at http://invitro.umassmed.edu/~sh/supplements/supplements.html) of the 45th z section of the cell shown in Fig. 1A (yellow outline). Since the full widths at half maximum of the intensity peaks shown in Fig. 1B (and in movie 1 at http://invitro.umassmed.edu/~sh/supplements/supplements.html) mostly exceed several micrometers, these large-scale PtdIns(4,5)P_2-rich membrane structures are clearly different from "membrane rafts," whose sizes are believed to be under the resolution of optical microscopy (>200 nm) (30). Instead, the physical sizes of these domains are close to or larger than those of membrane ruffles and phagosomal cups, within which PtdIns(4,5)P_2 enrichment has also been observed (6, 27). Thus, we designate these structures "membrane patches." In live adipocytes, we found PRMPs colocalized with membrane ruffles (yellow arrows in Fig. 1D) and in apparently thickened membrane regions (red arrow in Fig. 1D).

Recent evidence has surprisingly indicated that PtdIns(4,5)P_2-rich membrane domains may be caused entirely by membrane folds not resolved by fluorescence microscopy (13, 66). These findings challenge the concept that PtdIns(4,5)P_2 is laterally segregated in the 2D lipid bilayer. To test this possibility, we labeled live adipocytes expressing EGFP/PLCδ1-PH with Alx594-ConA and carried out time-dependent, dual-color deconvolution microscopic measurements (Fig. 2). Alx594-ConA has been used as a reagent for plasma membrane staining (7), and its fluorescence intensity was used as an indicator of local membrane density in this experiment (see below). We found that PRMPs in a cultured adipocyte undergo dynamic changes with (Fig. 2D and E) and without (Fig. 2A to C) insulin stimulation and that these changes closely mirror the dynamic distribution patterns for Alx594-ConA at the corresponding time points (Fig. 2F to J; see also movie 2 at http://invitro.umassmed.edu/~sh/supplements/supplements.html). The fact that PRMPs dynamically colocalize with membrane-rich domains stained with concentrated Alx594-ConA suggests that the apparent PtdIns(4,5)P_2 enrichments result at least partially from increases in local membrane content (see below) (66).

The time-dependent PRMP reorganization shown in Fig. 2 (and movie 2 at http://invitro.umassmed.edu/~sh/supplements/supplements.html) is associated with cellular morphology changes (i.e., the top portion of the cell expanded during image acquisition) but is not correlated with insulin stimulation. In fact, large-scale PRMP dynamics are not induced by insulin but are associated with dramatic changes in cellular morphology (see movie 3 at http://invitro.umassmed.edu/~sh/supplements/supplements.html). In contrast, most live adipocytes (i.e., >10 cells) examined by ultrafast-acquisition microscopy are sedentary and show no change in cell shape. Correspondingly, PRMPs are very stable (i.e., a half-life of >0.5 h) in these cells regardless of insulin stimulation (see movie 4 at http://invitro.umassmed.edu/~sh/supplements/supplements.html). How-

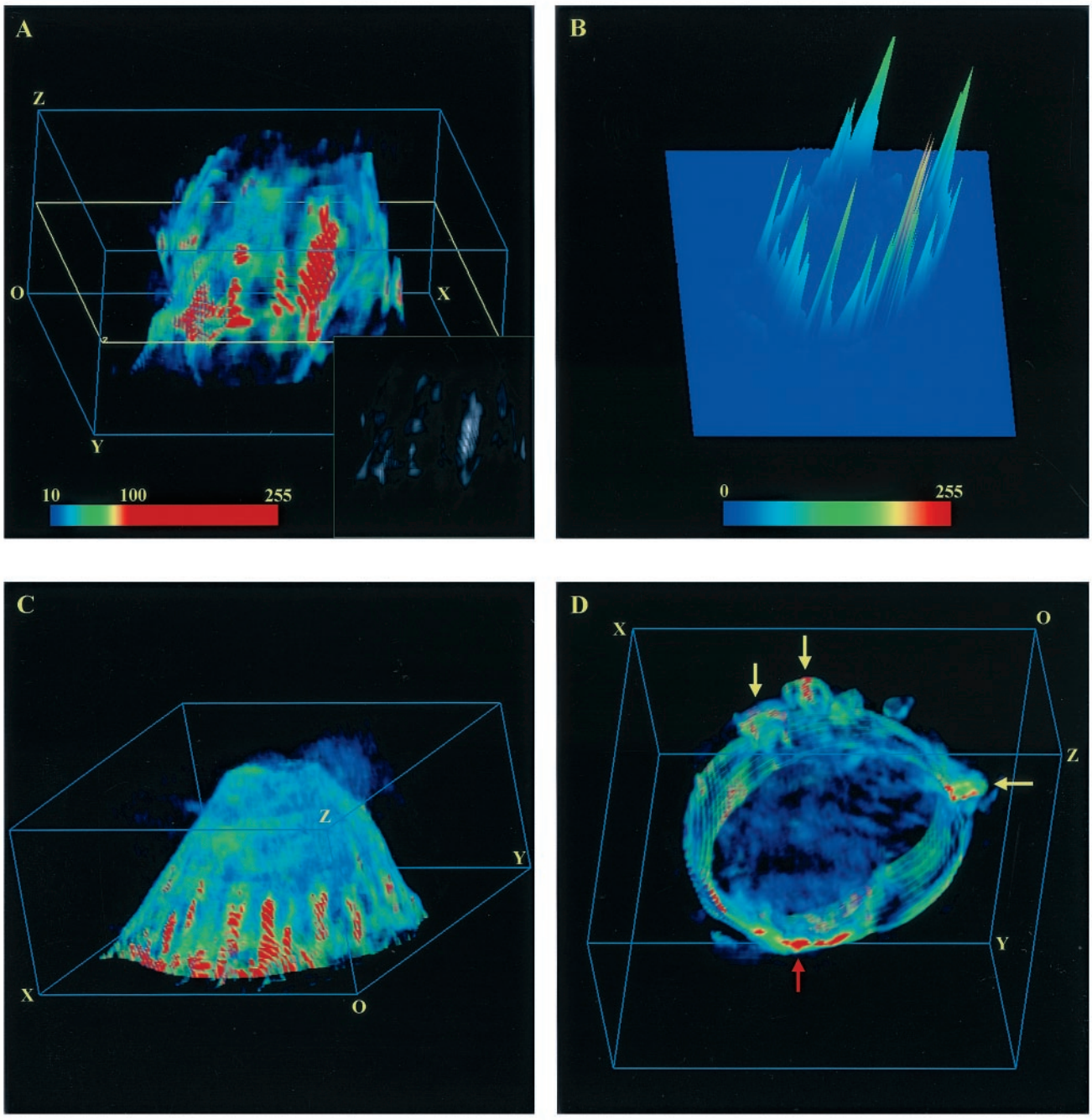

FIG. 1. Large-scale PRMPs on the surface of living 3T3-L1 adipocytes. (A, C, and D) 3D image stacks of adipocytes transiently expressing EGFP/PLCδ1-PH were acquired with an ultrafast-acquisition microscope (see Materials and Methods), and representative deconvolved images were projected within 3D grids measuring 42 by 43 by 20 μm. These cells are composed of 81, 81, and 30 *z* sections, respectively, which are stacked successively along the optical *z* axis. Each *z* section represents a 0.25-μm slice of cells. The cells are oriented in such a way that the bottom membranes attached to the coverslip are closest to the plane containing the origin (O). All cells were serum starved for >2 h, and the cell in panel C was subsequently insulin simulated for 10 min at 37°C. To facilitate visualization of the PtdIns(4,5)P_2 spatial distribution, the dynamic ranges (i.e., minimum to maximum pixel intensity ranges) of the original 12-bit images are linearly mapped to 8-bit false-color intensity scales. The images are further contrast enhanced between their respective background noise levels and 10 times above those levels (e.g., the false-color intensity scale bar in panel A). Thus, the image in panel A was rescaled at between 10 and 100, and those in panels C and D were rescaled at between 20 and 200. The resulting color images (e.g., panel A) were the first approximations of their 8-bit gray-scale counterparts without contrast enhancement (e.g., inset in panel A). Only the bottom section (i.e., *z*1 to *z*30) of the cell in panel D is shown; yellow arrows indicate membrane ruffles, while the red arrow indicates apparently thickened membrane regions. Ripple-like patterns in the 3D images (most apparent in the red regions in panels A and C) are related to the axial-to-lateral magnification ratio used for the ultrafast-acquisition microscope and should be regarded as continuous regions (see Materials and Methods).(B) Full-scale (i.e., 0 to 255) 8-bit 2D intensity plot of the 45th *z* section of the cell in panel A (yellow outline in panel A). (See movie 1 at http://invitro.umassmed.edu/~sh/supplements/supplements.html for a complete set of 2D intensity plots.)

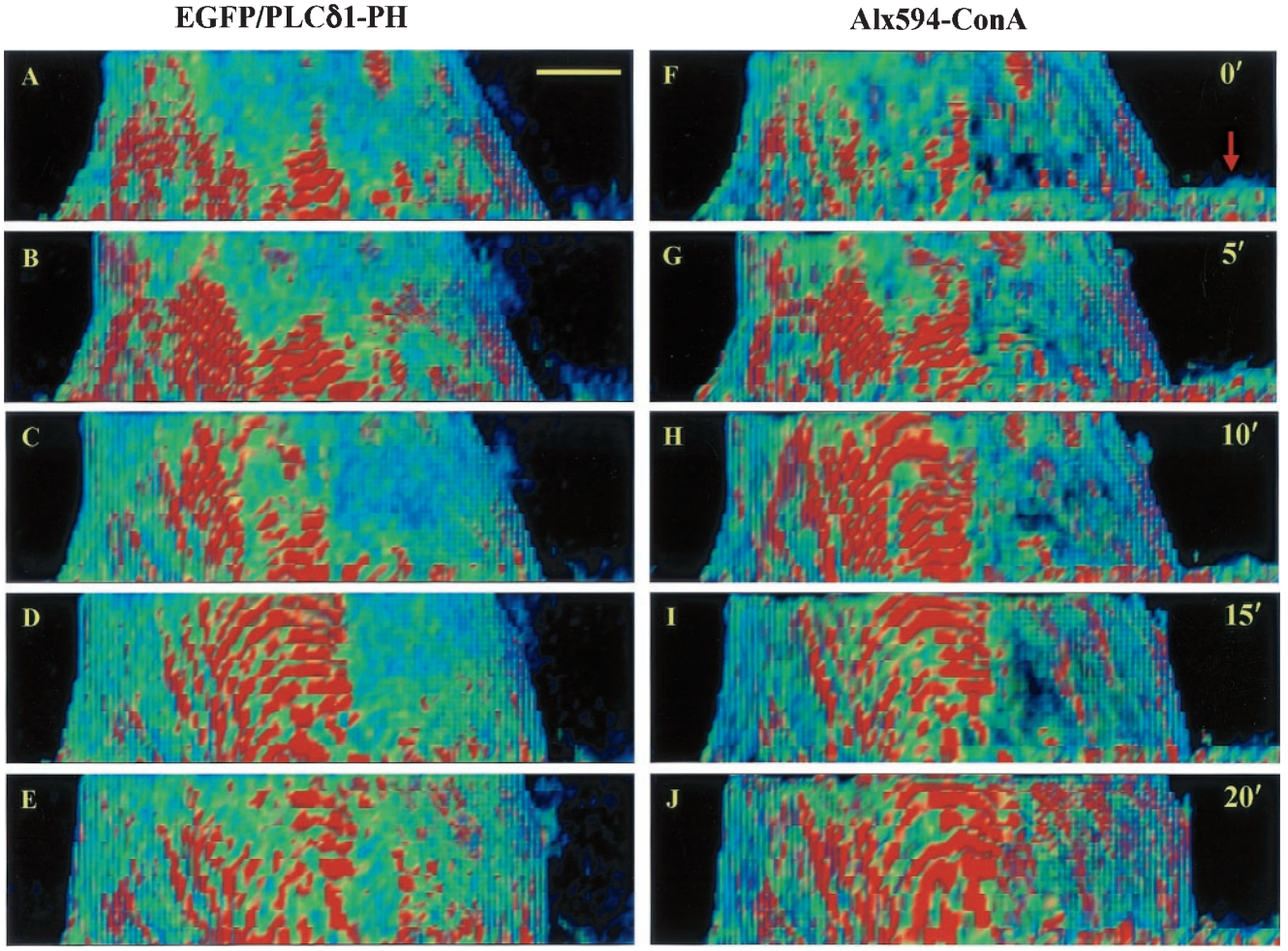

FIG. 2. PRMPs dynamically colocalize with lipid-dense plasma membrane domains on the surface of living adipocytes. The plasma membrane of a living adipocyte transiently expressing EGFP/PLCδ1-PH (A to E) was labeled with Alx594-ConA (F to J). Dual-color ultrafast-acquisition microscopy of this cell was carried out every 20 s for 20 min at 37°C. Image stacks consisting of 81 *z* sections were acquired with the EGFP and Alx594 fluorescence channels in an interlaced fashion, with the corresponding *z* sections in these two channels being acquired sequentially and separated by ~5 ms. Only side views of the plasma membrane are shown at representative time points (e.g., A and F at 0 min), and 100 nM insulin was added at 10 min (i.e., immediately after C and H). Deconvolved false-color images acquired with the EGFP (A to E) and Alx594 (F to J) fluorescence channels were rescaled between 10 and 100 and between 6 and 60, respectively (Fig. 1). The arrow in panel F indicates part of a fibroblast in the foreground of panels F to J; this fibroblast is labeled with Alx594-ConA but does not express EGFP/PLCδ1-PH. Scale bar, 5 μm.

ever, the ultrafast-acquisition microscopy technique used here sacrifices resolution for speed (see Materials and Methods) and may miss structural changes occurring on smaller spatial scales (35). Therefore, structural details associated with PRMPs were further examined in fixed adipocytes (see Fig. 5, 7 to 9, and 12) by using high-magnification (i.e., 66 nm/pixel) imaging combined with a superresolution deconvolution algorithm, which achieves a lateral resolution approaching ~100 nm (11). Alternatively, the frequency and size of membrane ruffles can be enhanced by overexpression of unconventional Myo1c, thus enabling real-time examination of their spatial relationship to PRMPs (see Fig. 13; see also movie 8 at http://invitro.umassmed.edu/~sh/supplements/supplements.html).

Mechanisms of PtdIns(4,5)P_2 enrichment in PRMPs. To further investigate the mechanisms that concentrate PtdIns(4,5)P_2 in PRMPs, we carried out a quantitative ratiometric analysis (see Materials and Methods) of images of doubly-labeled adipocytes (Fig. 3 and 4). Three membrane-staining reagents, DiIC18, BODIPY-HPC, and Alx594-ConA, were tested for their suitability for indicating local lipid or membrane density. The former two are lipophilic dyes that are preferentially partitioned into lipid-ordered and lipid-fluid phases, respectively (37), and the latter mostly binds to cell surface glycoproteins. Surprisingly, only 57% of live adipocytes (34 out of 60) are stained with DiIC18, and the percentage decreases to 35% for cells expressing EGFP/PLCδ1-PH (19 out of 54). The significance of these results is not clear yet. However, since DiIC18 has been shown to stain a variety of cells (36, 66), this observation does indicate that the lipid composition of the adipocyte plasma membrane is unique in that it partially excludes DiIC18 labeling.

In contrast, it was found that both BODIPY-HPC and Alx594-ConA stain all 3T3-L1 adipocytes, whether or not the cells express EGFP/PLCδ1-PH. Single-plane images of live

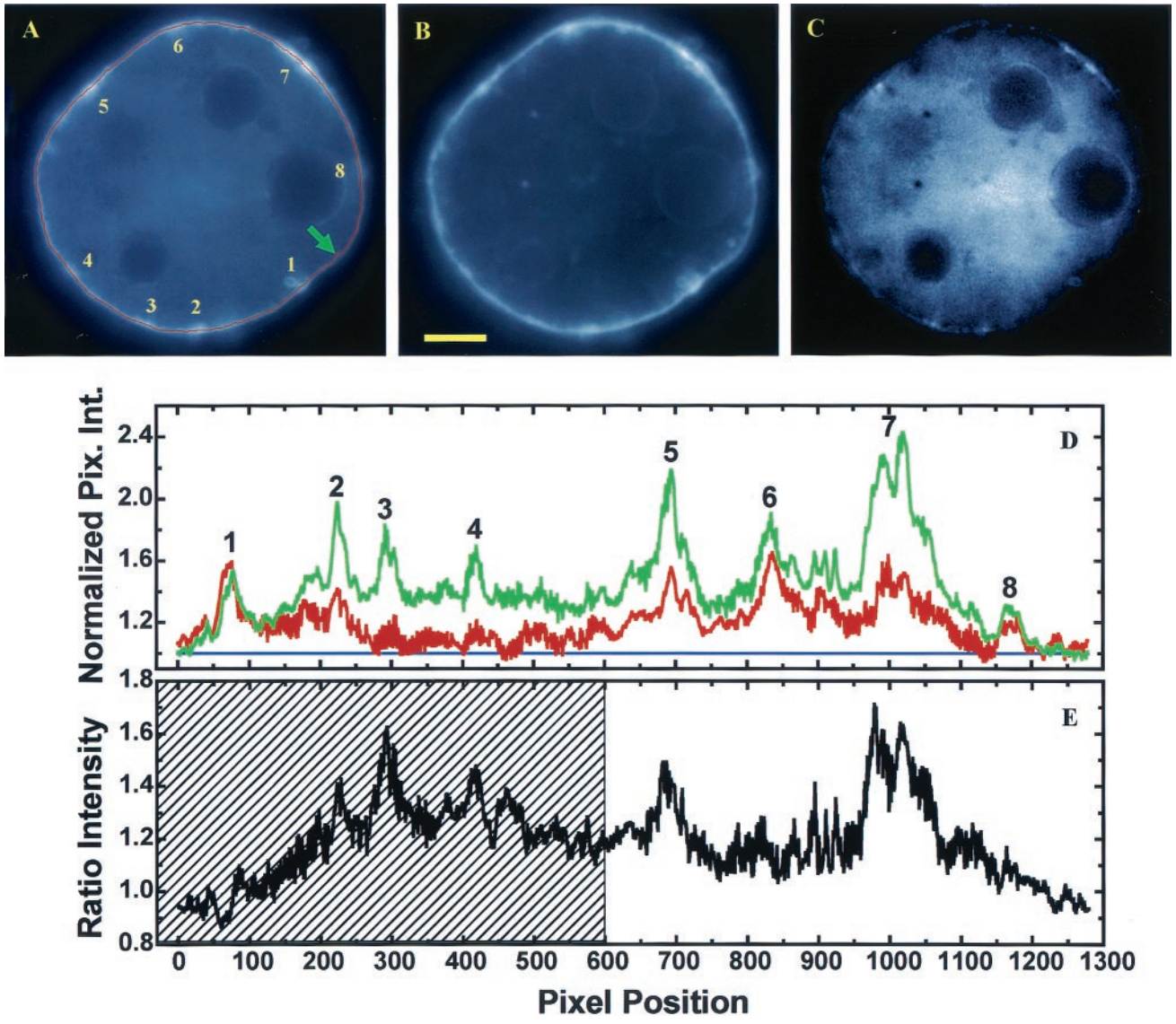

FIG. 3. Quantitative image analysis of a live adipocyte expressing EGFP/PLCδ1-PH (A) and labeled with the membrane-staining dye BODIPY-HPC (B). A deformable snake algorithm (71) was used to automatically find the cellular boundary (shown only in panel A as a red line). (D) Plot of normalized fluorescence intensities (i.e., $I'_{EGFP} = I_{EGFP}/IGM_{EGFP}$ and $I'_{BODIPY} = I_{BODIPY}/IGM_{BODIPY}$; see Results) along the cell boundary (green line, EGFP/PLCδ1-PH fluorescence; red line, BODIPY-HPC fluorescence). Pix. Int., pixel intensity. Blue line, baseline. (E) Ratiometric intensities (i.e., I'_{EGFP}/I'_{BODIPY}). (C) Corresponding 14-bit ratiometric image [i.e., panel C = (panel A · 10^4)/(panel B · NF)]. The normalization factor (NF) is defined as IGM_{EGFP}/IGM_{BODIPY}. The image in panel C was further rescaled at between 10^4 and the maximum pixel intensity so that only an I_{EGFP}/I_{BODIPY} ratio >1 is visible. Peak EGFP fluorescence intensities corresponding to PtdIns(4,5)P_2-rich membrane domains are labeled 1 to 9 in panels A and D. However, the cross-hatched region in panel E could also represent a broad peak. The arrow in panel A indicates the starting point of the line intensity profile (clockwise). BODIPY-HPC staining was carried out at 0°C, and images were acquired at 8 to 10°C to inhibit constitutive endocytosis. Scale bar, 5 μm.

cells obtained with both the EGFP (Fig. 3A) and the BODIPY-HPC (Fig. 3B) fluorescence channels show little fluorescence bleaching. With this method, only fluorescence variations within the in-focus plane (i.e., a plane with a thickness of ~1.0 μm for a 1.40-NA oil objective) are resolved, and out-of-focus fluorescence contributes to a mostly smooth background (53). Measurements were obtained for 20 cells, and a representative example is shown in Fig. 3. A deformable snake algorithm (71) was used to automatically find the cellular boundary (red line in Fig. 3A), which consists of peripheral pixels of the cell with the highest local intensities. The resulting boundary derived from the EGFP fluorescence image (Fig. 3A) was applied without change to the BODIPY-HPC image (Fig. 3B). The fluorescence intensities of five pixels (i.e., one on the cell boundary and its two nearest neighbors on either side of the boundary) were averaged to account for the apparent thickness of the plasma membrane. Almost identical intensity profiles were obtained when the averaging was done over one, five, or nine pixels (data not shown), indicating that the apparent membrane thickness does not interfere with the data

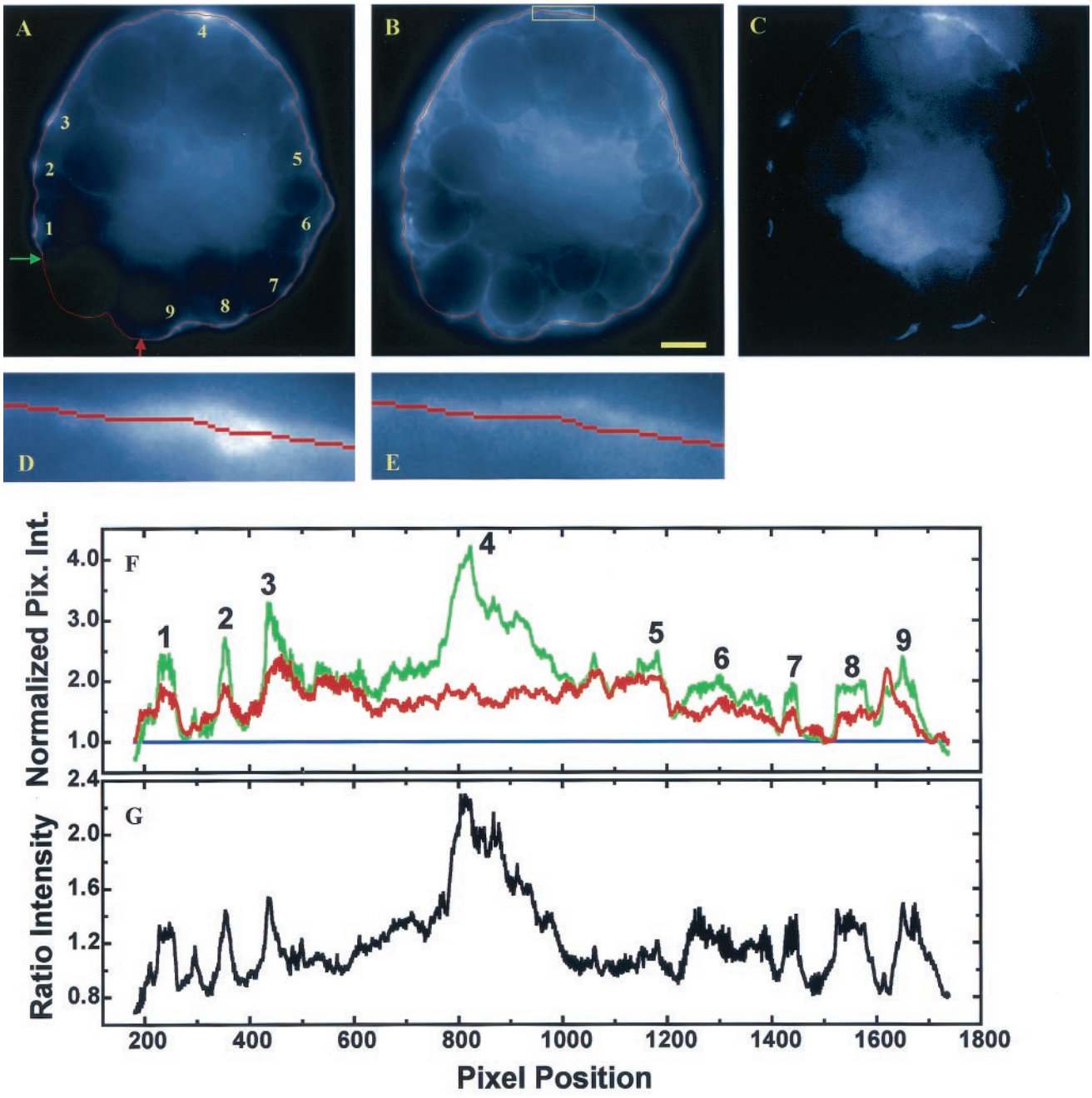

FIG. 4. Quantitative image analysis of a fixed adipocyte expressing EGFP/PLCδ1-PH (A) and labeled with the membrane-staining probe Alx594-ConA (B). (F) Plot of normalized fluorescence intensities (green line, EGFP fluorescence; red line, Alx594 signal) along the cell boundary (i.e., red lines in panels A and B). Pix. Int., pixel intensity. Blue line, baseline. (C and G) Ratiometric intensities (G) and corresponding ratiometric image (C) generated as described in the legend to Fig. 3. (D and E) Magnified views of the boxed regions (box shown only in panel B) in panels A and B, respectively. Peak EGFP fluorescence intensities corresponding to PtdIns(4,5)P_2-rich membrane domains are labeled 1 to 9 in panels A and F. Green and red arrows in panel A indicate the starting and ending points of the line intensity profile (clockwise), respectively. Consequently, a portion of the cell boundary suspected of being broken is excluded from data analysis. Scale bar, 5 μm.

analysis. The EGFP and BODIPY-HPC fluorescence intensities (I_{EGFP} and I_{BODIPY}, respectively) are normalized to their respective global minimums (IGMs) and are plotted in Fig. 3D. Since membrane regions associated with IGMs are the least likely places for both membrane folding and lateral PtdIns(4,5)P_2 segregation, the normalized BODIPY signal (i.e., $I'_{BODIPY} = I_{BODIPY}/IGM_{BODIPY}$) reflects the relative degree of local membrane density elsewhere, while the normalized EGFP signal (i.e., $I'_{EGFP} = I_{EGFP}/IGM_{EGFP}$) accounts for both local membrane density and additional lateral PtdIns(4,5)P_2 accumulation in the 2D lipid bilayer. Consequently, $\Delta I' = [(I'_{EGFP} - I'_{BODIPY})] \times 100$ is a good approximation of local PtdIns(4,5)P_2 enrichment beyond what can be accounted for by an increase in local membrane content (see

Materials and Methods). In addition, the normalization procedure also accounts for different levels of expression of EGFP/PLCδ1-PH in individual cells.

From Fig. 3D, it is clear that PtdIns(4,5)P_2-rich (i.e., EGFP/PLCδ1-PH labeling; green line) and lipid-dense (i.e., BODIPY-HPC labeling; red line) membrane domains (labeled 1 to 8 in Fig. 3A and D) exclusively colocalize, a finding which is also apparent from a comparison of the fluorescence images in Fig. 3A and B. This colocalization is found in all 20 cells examined and reaffirms the conclusion derived from Fig. 2 that PtdIns(4,5)P_2 is enriched in the 3D space of PRMPs through a mechanism involving local membrane folding. Furthermore, except for domain 1, peak EGFP fluorescence intensities are all higher than their BODIPY-HPC counterparts. An average $\Delta I'$ of 45% ± 10% (mean and standard error of the mean) was obtained for all eight peaks, indicating additional PtdIns(4,5)P_2 enrichment in the PRMPs beyond the increase in local membrane density. However, it was also observed that I'_{EGFP} is globally higher than I'_{BODIPY}, except in the vicinity surrounding peaks 1 and 8. In fact, the average EGFP intensity is 23% ± 1% higher than that of its BODIPY-HPC counterpart. These results could suggest that a nonlinear baseline instead of the linear baseline depicted in Fig. 3D (blue line) should be used to estimate relative peak heights. Thus, a peak height should be defined by the baseline established by its associated valleys. To test this hypothesis, a ratiometric intensity profile (I'_{EGFP}/I'_{BODIPY}), which is independent of the methods of fluorescence normalization (see above), is plotted in Fig. 3E. It clearly shows, for peaks 2, 3, 5, and 7, higher magnitudes of EGFP fluorescence above the noisy baselines surrounding these peaks (Fig. 3E). This effect is best visualized in the ratiometric image (Fig. 3C), in which the higher EGFP/PLCδ1-PH intensities are clearly visible above the background noise. Finally, the exact value of $\Delta I'$ is dependent on how a fluorescence peak is defined. For example, the cross-hatched region in Fig. 3E can be regarded as a broad peak. In this case, the calculated $\Delta I'$ will be between 23% ± 1% and 45% ± 10%.

The above-mentioned considerations demonstrate that the average $\Delta I'$ of 45% ± 10% should be regarded as the upper limit of lateral PtdIns(4,5)P_2 enrichment in PRMPs. Similarly, an average upper limit of 46% ± 13% was calculated from a total of 55 PRMPs examined for four representative cells. However, quantitative analysis (Fig. 3) assumes that there is no interaction between the BODIPY-HPC and EGFP/PLCδ1-PH labels, because the data (Fig. 3) can also be explained by a nonlinear exclusion mechanism, in which a higher local level of EGFP/PLCδ1-PH progressively inhibits BODIPY-HPC labeling. Therefore, we tested another fluorescent probe that binds to the plasma membrane via a different mechanism (see below).

ConA binds to oligosaccharide residues on the outer leaflet of plasma membranes, while EGFP/PLCδ1-PH targets PtdIns(4,5)P_2 on the inner leaflet. Therefore, these two membrane probes should not interfere with each other. Furthermore, unlike lipophilic dyes, ConA can be effectively cross-linked in formaldehyde-fixed samples. Thus, fluorescently labeled ConA is the reagent of choice for subsequent super-resolution deconvolution microscopic studies of fixed adipocytes (Fig. 5 to 9). However, ConA can only indirectly probe local lipid density through its interaction with membrane-bound glycoproteins. Thus, we found various degrees of spatial divergence between the ConA- and EGFP/PLCδ1-PH-rich membrane domains in fixed adipocytes. Nevertheless, where these two probes completely colocalize in the plasma membrane (Fig. 4), we found that the normalized Alx594-ConA and EGFP/PLCδ1-PH intensity profiles are well aligned (Fig. 4F). That is, differences in fluorescence intensities occur only in the peak positions (labeled 1 to 9 in Fig. 4A and F), and the valleys associated with these peaks overlap (Fig. 4F). Therefore, additional PtdIns(4,5)P_2 enrichment occurs only in PRMPs. The average $\Delta I'$ was calculated to be 48% ± 8% (excluding peak 4); this value agrees very well with the average $\Delta I'$ of 46% ± 13% estimated with BODIPY-HPC as the membrane stain (Fig. 3). These results, together with the ratiometric intensity profile (Fig. 4G) and the ratiometric image (Fig. 4C), indicate that there is additional PtdIns(4,5)P_2 enrichment in PRMPs above that accounted for by an increase in local membrane content. Taken together, the results derived from Fig. 3 and 4 support a mechanism in which PtdIns(4,5)P_2 is somehow concentrated in the lipid bilayer of PRMPs in addition to its increased concentration in 3D space due to local membrane folding.

We noted that peak 4 in Fig. 4 is unique in that it has a high EGFP/PLCδ1-PH fluorescence intensity but no corresponding spike in Alx594-ConA labeling. This is because the deformable snake algorithm localizes the maximum local EGFP fluorescence (Fig. 4D) to just beneath the plasma membrane defined by extracellular Alx594-ConA labeling (Fig. 4E). Thus, fluorescence signals associated with these two reporters do not colocalize exactly in this region. The PtdIns(4,5)P_2-containing structures immediately beneath the plasma membrane were examined in detail in Fig. 7 to 9.

The data reported above indicate that PRMPs are PtdIns(4,5)P_2- and membrane-rich structures on the adipocyte cell surface. The estimated upper limit of 46% ± 13% for PtdIns(4,5)P_2 enrichment in PRMPs (Fig. 3) above the increase in the general membrane material content agrees well with the reported ~40% higher PtdIns(4,5)P_2 concentration in the membranes of phagosomal cups (6). In the latter study, local membrane density was controlled for by myristoylated GFP localized to the plasma membrane, and fluorescence images obtained with a confocal microscope were used for quantitative analysis. These results are also consistent with quantitative electron microscopic studies indicating that PtdIns(4,5)P_2 is enriched in the lamellipodia of HEK-293 astrocytoma cells (68). Taken together, converging lines of evidence based on different techniques have confirmed the concept that PtdIns(4,5)P_2 can be laterally segregated in micrometer-sized domains in 2D lipid bilayers. Interestingly, both the results of phagocytosis studies and the results derived from Fig. 3 and 4 indicate that such lateral segregation preferentially occurs at the same sites at which local membrane folds concentrate PtdIns(4,5)P_2 in 3D space.

PRMPs colocalize exclusively with regions of dense cortical F actin. Directing actin polymerization is one of the major and best-characterized signaling functions of PtdIns(4,5)P_2 (10, 32, 54, 58). We therefore examined the spatial relationship between PRMPs and the underlying actin cytoskeleton (Fig. 5). In a three-color colocalization study, PtdIns(4,5)P_2 localization is revealed by a fusion protein linking ECFP to the PH domain

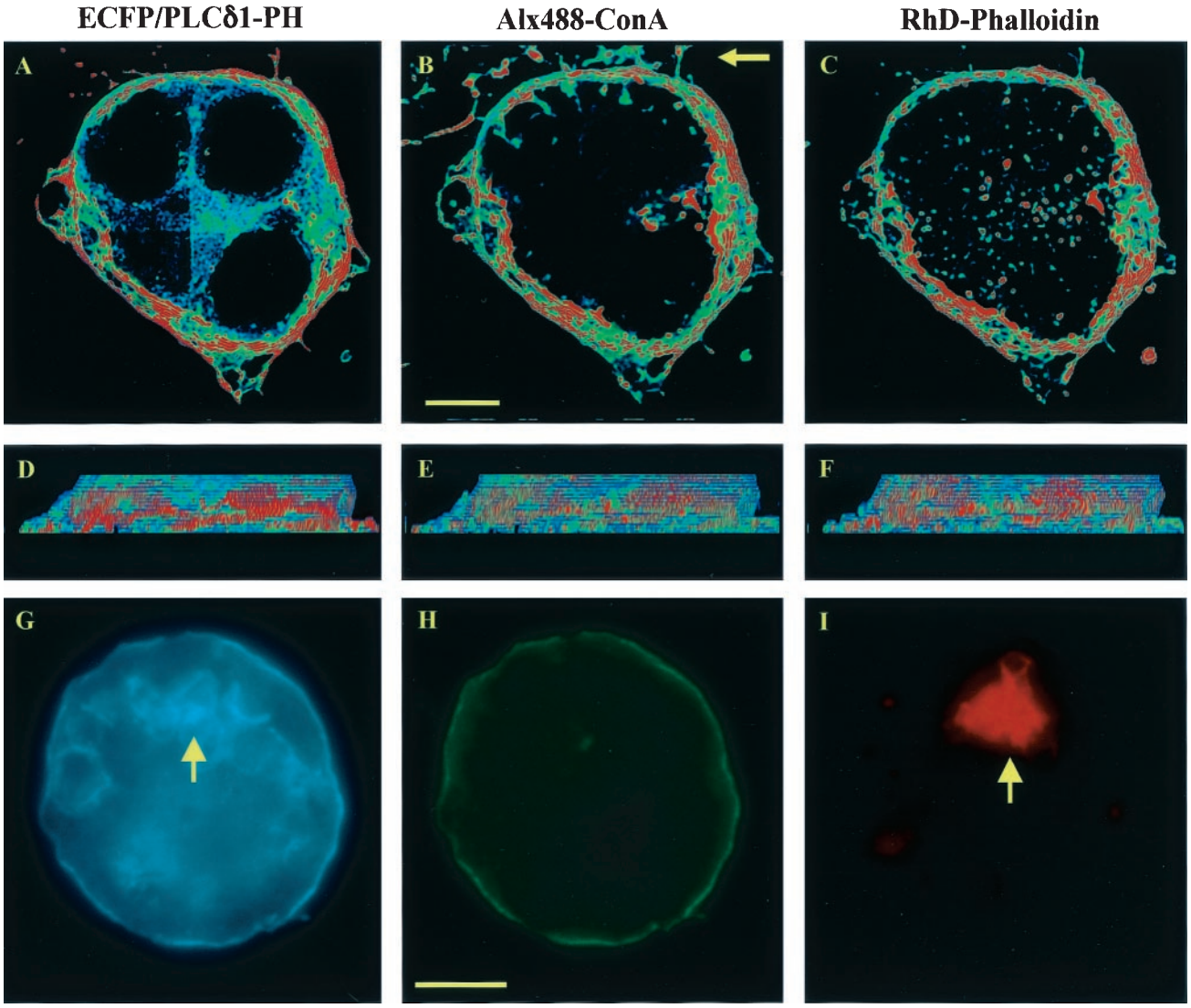

FIG. 5. PRMPs associate exclusively with regions of dense cortical F-actin. Adipocytes expressing ECFP/PLCδ1-PH (A, D, and G) were fixed and labeled with Alx488-ConA for the plasma membrane (B, E, and H), followed by cell permeabilization and F-actin staining with RhD-PhD (C, F, and I). High-magnification (i.e., 66 nm/pixel) image stacks consisting of 17 *z* sections were acquired with negligible cross talk among the three fluorescence channels (see Materials and Methods) and were processed with a superresolution deconvolution algorithm (11). Distribution patterns for the fluorescent probes (A to F) were visualized with 8-bit false-color intensity scales and were contrast enhanced at between 10 and 100 for panels A and D, between 10 and 70 for panels B and E, and between 10 and 50 for panels C and F. The cell is viewed both from the top (A to C) and from the side (D to F; the side indicated by the arrow in panel B). In addition, single-plane images of an adipocyte expressing ECFP/PLCδ1-PH at a high level (i.e., intracellular aggregates of the fusion protein indicated by the arrow in panel G) are shown in panels G to I with 8-bit single-color intensity scales (cyan, ECFP/PLCδ1-PH; green, Alx488-ConA; red, Rhd-Phd). The cell shown in panels G to I is accessible to Rhd-Phd labeling, as indicated by the intracellular RhD fluorescence (arrow in panel I). Adipocytes were serum starved for >2 h, and the cell in panels G to I was subsequently insulin stimulated at 37°C for 10 min. Scale bars, 5 μm.

of PLCδ1 (ECFP/PLCδ1-PH). ECFP/PLCδ1-PH shows the same binding specificity for PtdIns(4,5)P_2 on the plasma membrane (Fig. 5A and 9A) as EGFP/PLCδ1-PH, and a mutant form of ECFP/PLCδ1-PH deficient in PtdIns(4,5)P_2 binding (i.e., R40L) displays uniform fluorescence distribution in the cytoplasm (data not shown). A fully differentiated adipocyte (i.e., day 7 differentiation) (35) transiently expressing ECFP/PLCδ1-PH (Fig. 5A and D) was fixed and subsequently labeled with Alx488-ConA to reveal the plasma membrane (Fig. 5B and E), followed by cell permeabilization and Rhd-Phd staining to visualize cortical F actin (Fig. 5C and F). High-magnification (i.e., 66 nm/pixel) image stacks were acquired and processed with a superresolution deconvolution algorithm that is capable of resolving structural details at ~100 nm (11). Distribution patterns for the three fluorescent labels were visualized with 8-bit false-color intensity scales and showed a striking resemblance to each other when viewed from the top (Fig. 5A to C) or side (Fig. 5D to F) of the cell. This exclusive colocalization between PRMPs and regions of dense cortical F actin is found in dozens of serum-starved adipocytes (e.g., Fig. 5A to F) and insulin-stimulated adipocytes (data not shown), suggesting that PRMPs may direct the spatial organization of

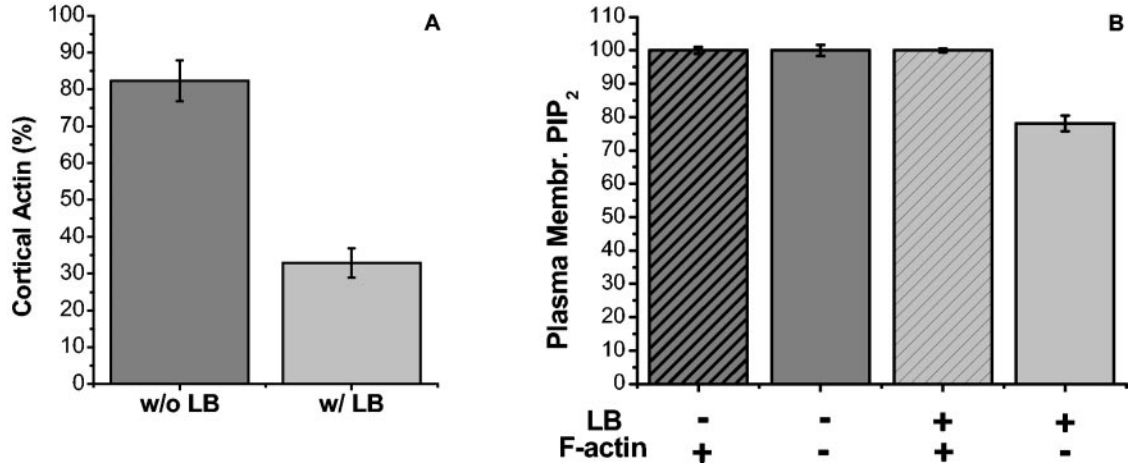

FIG. 6. Display of PtdIns(4,5)P_2 in the plasma membrane of 3T3-L1 adipocytes is independent of the cortical F-actin cytoskeleton. Morphologically differentiated adipocytes (day 7) expressing EGFP/PLCδ1-PH were serum starved for >2 h. A portion of the cells was incubated with 60 μM LB for 2 h at 37°C. The cells were fixed in 4% formaldehyde, followed by Rhd-Phd staining for F actin (Fig. 5). (A) Percentages of cells displaying at least partial cortical F actin (i.e., F-actin positive) with (w/) or without (w/o) LB treatment. PtdIns(4,5)P_2 production was monitored by the plasma membrane localization of EGFP/PLCδ1-PH. (B) Percentages of cells with plasma membrane (Membr.) PtdIns(4,5)P_2 (PIP_2) as a function of LB treatment and intactness of cortical F-actin. Error bars are standard errors of the mean from two independent experiments. [See movie 5 at http://invitro.umassmed.edu/~sh/supplements/supplements.html for the distribution of PtdIns(4,5)P_2 on the surfaces of two adipocytes completely devoid of F actin.]

the cortical cytoskeleton. This hypothesis is consistent with the observation that drastic overexpression of ECFP/PLCδ1-PH, as indicated by the intracellular aggregation of the fusion protein (arrow in Fig. 5G), prevents cortical F-actin formation in both serum-starved cells (data not shown) and insulin-stimulated cells (Fig. 5G to I, 10, and 11). That this effect is specific is confirmed by the fact that Alx488-ConA staining of the outer leaflet of the plasma membrane is not visibly affected (Fig. 5H). In contrast, cortical F-actin formation relies on the direct accessibility of PtdIns(4,5)P_2 on the inner leaflet of the plasma membrane, which is blocked by the overexpression of ECFP/PLCδ1-PH (Fig. 5I).

The exclusive colocalization between PRMPs and regions of dense F-actin (Fig. 5) prompted us to address whether the plasma membrane localization of PtdIns(4,5)P_2 and PRMP formation are dependent on actin polymerization. It was previously reported (35) and confirmed in the present studies that a layer of cortical F-actin is formed in fully differentiated 3T3-L1 adipocytes. For example, at day 7 of differentiation, 82% ± 5% (Fig. 6A) of cultured adipocytes possess distinct cortical F-actin upon Rhd-Phd staining (Fig. 5A to F). Incubation of these cells with the actin polymerization inhibitor LB severely disrupts F-actin formation (Fig. 6A). However, in 32% ± 4% of these LB-treated cells, some of the F-actin cytoskeleton is preserved. The presence of cortical F-actin in these fully differentiated adipocytes and its disruption by LB are not dependent on acute insulin stimulation (35), although insulin can enhance the formation of additional F-actin in serum-starved adipocytes (33). In a population (i.e., ~18%) of unstimulated adipocytes that do not show distinct cortical F-actin, we found that all adipocytes expressing EGFP/PLCδ1-PH have clear plasma membrane localization of the fusion protein (Fig. 6B). Thus, without LB treatment, display of PtdIns(4,5)P_2 on the plasma membrane is independent of insulin stimulation and the cortical cytoskeleton. In LB-treated cells, 100% ± 1% adipocytes with at least some cortical F-actin display plasma membrane localization of EGFP/PLCδ1-PH, and the percentage decreases to 78% ± 2% in cells that are completely devoid of F actin (Fig. 6B). This result is likely due to the potential toxicity of LB for a kinase(s) that synthesizes PtdIns(4,5)P_2 in cells that take up large amounts of this drug. Overall, however, PtdIns(4,5)P_2 localization to the plasma membrane is largely independent of cortical F-actin formation.

High-magnification optical sections of four LB-treated adipocytes expressing EGFP/PLCδ1-PH but completely devoid of F-actin were acquired and deconvolved with the superresolution deconvolution algorithm. PRMPs still form in these cells (see movie 5 at http://invitro.umassmed.edu/~sh/supplements/supplements.html) and are qualitatively indistinguishable (in three out of four cells) from those observed in control live or fixed cells (Fig. 1, 2, 5, 7, 9, 12, and 13). Live adipocytes that did not undergo the electroporation process were also labeled with Alx594-ConA. These cells were quickly fixed and examined with the superresolution deconvolution imaging technique. An elaborate PRMP-like network is found on the surface of these cells (see movie 6 at http://invitro.umassmed.edu/~sh/supplements/supplements.html), indicating that PRMPs are not artifacts of EGFP/PLCδ1-PH expression and/or the electroporation process. Thus, both PtdIns(4,5)P_2 localization to the plasma membrane and PRMP formation are independent of cortical F-actin formation. Instead, uneven distribution of plasma membrane content is an intrinsic property of 3T3-L1 adipocytes and other cell lines (see Discussion) and is the major mechanism contributing to PRMP formation (Fig. 2 to 4).

PtdIns(4,5)P_2-containing vesicular structures beneath PRMPs. It has long been established that PtdIns(4,5)P_2 plays a crucial role in clathrin-assisted endocytosis by recruiting multiple molecular components to the plasma membrane (14, 22, 43). Subsequent PtdIns(4,5)P_2 hydrolysis on the nascent endo-

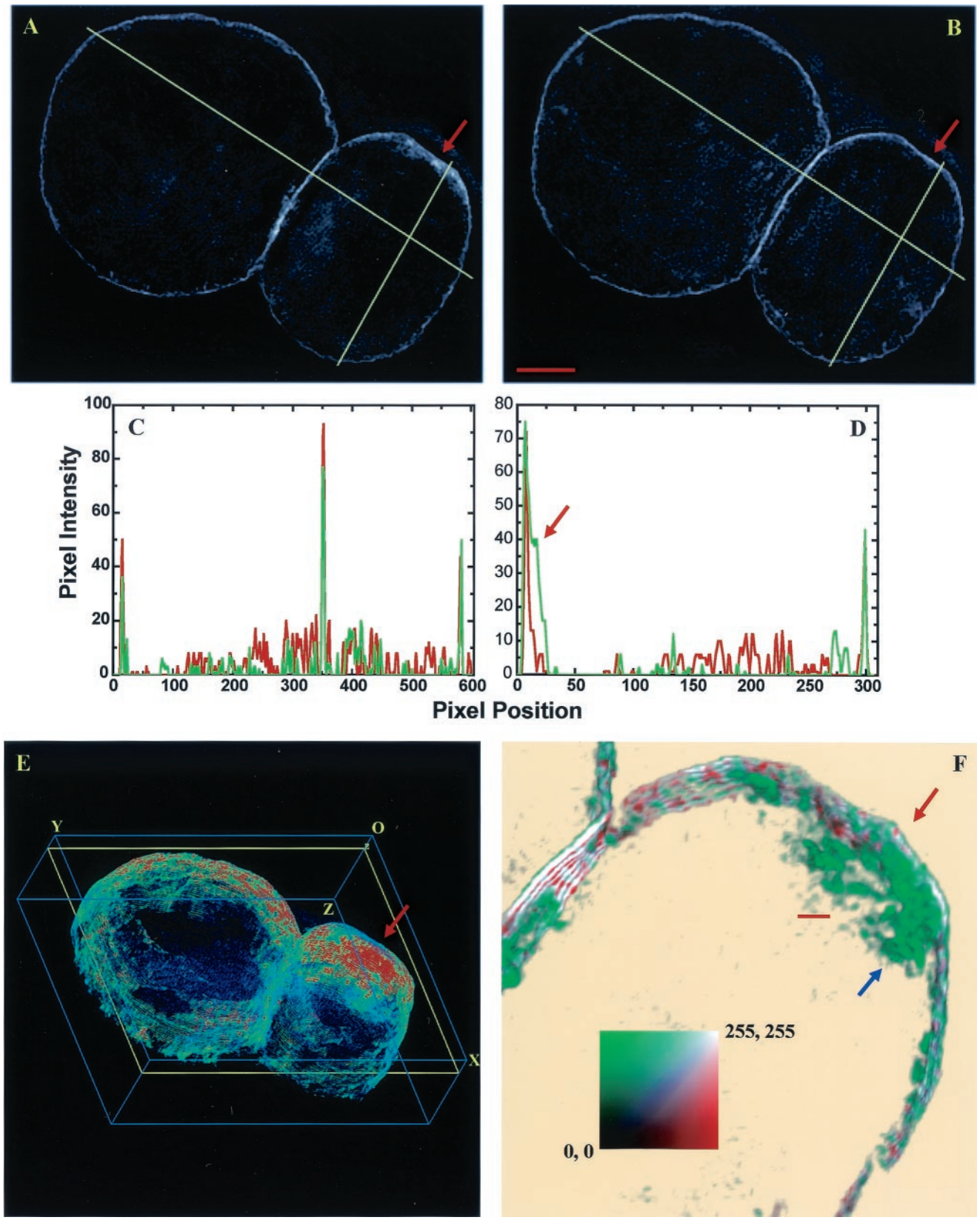

FIG. 7. PtdIns(4,5)P_2-containing vesicular structures just beneath the PRMP of a fixed adipocyte. (A, B, and E) Two adipocytes transiently expressing EGFP/PLCδ1-PH (A and E) were labeled with Alx594-ConA (B) after cell fixation. The dynamic range of the deconvolved 3D image obtained with the EGFP fluorescence channel (E) was mapped to an 8-bit false-color intensity scale and contrast enhanced at between 10 and 100. The images in panels A and B are the 17th *z* sections of their respective 3D deconvolved images. The dimensions of the 3D grid in panel E are

somes is believed to be important for the clathrin coat disassembly that precedes endosome maturation toward the interior of a cell or recycling back to the plasma membrane (22). However, this dynamic process of PtdIns(4,5)P_2 turnover has not been directly observed. We hypothesized that the PtdIns(4,5)P_2-containing structures found beneath the plasma membrane (e.g., peak 4 in Fig. 4) are related to adipocyte endocytic activities. Therefore, these structures were examined in further detail by superresolution deconvolution microscopy in Fig. 7 to 9.

Figure 7 shows two adjoining adipocytes, both expressing EGFP/PLCδ1-PH (Fig. 7A) and labeled with Alx594-ConA (Fig. 7B) after cell fixation. Intensity profiles for lines drawn across the two cells or the right-side cell alone are plotted in Fig. 7C and D, respectively (green line, EGFP/PLCδ1-PH labeling; red line, Alx594-ConA staining). Because of the resolution limit (i.e., >200 nm) of optical microscopy, the center plasma membranes attaching the two cells appear as a single fluorescence entity (Fig. 7A to C). As expected, the fluorescence intensities associated with these center membranes are approximately double those of the single plasma membranes on the other sides of these cells (Fig. 7C). This result indicates that Alx594-ConA is a sensitive indicator of local membrane density and that the local PtdIns(4,5)P_2 concentration is approximately proportional to the total lipid content in these membrane regions. In contrast, the right-side cell appears to be polarized, with one side of the plasma membrane being enriched in both PtdIns(4,5)P_2 and overall lipid contents (i.e., a PRMP) (red arrows in Fig. 7). Furthermore, the PRMP, when visualized with EGFP/PLCδ1-PH fluorescence (Fig. 7A), appears to be thicker than its Alx594-ConA-labeled counterpart (Fig. 7B). Correspondingly, there is an additional shoulder associated with the EGFP/PLCδ1-PH peak (arrow in Fig. 7D) at ~1 μm beneath the cell boundary defined by both EGFP/PLCδ1-PH and Alx594-ConA labeling (left peaks in Fig. 7D). To resolve these additional PtdIns(4,5)P_2-containing structures, superresolution deconvolution images were acquired at a lateral resolution of ~100 nm (Fig. 7E and F) (11). The deconvolved 3D image in Fig. 7E (EGFP fluorescence only) shows that the PRMP extends throughout one side of the cell (red arrow). Furthermore, in the colocalization image (Fig. 7F; colocalized regions are white), a magnified view of a 1.5-μm slice of that PRMP (yellow outline in Fig. 7E), shows vesicle-like, PtdIns(4,5)P_2-rich structures (green) just beneath the plasma membrane defined by extracellular Alx594-ConA staining (red). Within the resolution of the microscopic technique, these "vesicles" are ~100 to 300 nm in diameter and appear to be interconnected and partially attached to the plasma membrane (blue arrow in Fig. 7F). In contrast, no similar PtdIns(4,5)P_2-containing membranes are found further inside the cells (Fig. 7). This proximity of PtdIns(4,5)P_2-containing "vesicles" to PRMPs is found in three out of four adipocytes examined in the superresolution fashion, suggesting that PRMPs may spatially organize endocytic activities (see below).

The dynamic nature of these PtdIns(4,5)P_2-containing "vesicles" is revealed by differential Alx594-ConA staining before (Fig. 8B to D) and after (Fig. 8A) adipocyte fixation. Because surface Alx594-ConA is continuously internalized, various stages of the endocytosis process can be immobilized in fixed adipocytes so that structural details can be resolved later by superresolution deconvolution microscopy. The difference in Alx594-ConA staining of living and fixed adipocytes is most apparent for the bottom membranes attached to coverslips (0.75-μm *z* sections) (Fig. 8A and B). When Alx594-ConA (red regions in Fig. 8B) is applied to living adipocytes at 37°C, the probe is able to label lipid-rich structures on the bottom membrane together with EGFP/PLCδ1-PH (green regions in Fig. 8B). On the other hand, Alx594-ConA cannot diffuse to the bottom membrane after cell fixation, and only EGFP/PLCδ1-PH is present there (Fig. 8A). When live cells are stained, the process of Alx594-ConA internalization appears to be manifested initially as endocytic vesicles containing both EGFP/PLCδ1-PH and Alx594-ConA (Fig. 8C; colocalized regions are white) and lining the inner surface of the plasma membrane (green arrows in Fig. 8C). It also appears that, when these endocytic membranes mature toward the interior of the cell, the Alx594-ConA label progressively dominates (green arrows in Fig. 8C). Importantly, only Alx594-ConA persists on the intracellular vesicles (cyan arrowheads in Fig. 8C). This apparent maturation process is most obvious in a magnified region (i.e., a 1-μm-thick *z* section) of another adipocyte showing massive endocytic activities, where "vesicles" containing only Alx594-ConA appear to emerge from the tip of this membrane trafficking event while "vesicles" still containing EGFP/PLCδ1-PH are closer to and partially attached to the plasma membrane (Fig. 8D). Taken together, the data presented in Fig. 7 and 8 are consistent with the hypothesis that PtdIns(4,5)P_2 is lost from endocytic membranes early in the endocytosis process (15, 22).

PRMPs colocalize with active zones of clathrin-assisted endocytosis. To establish a direct link between the PtdIns(4,5)P_2-containing "vesicles" and clathrin-assisted endocytosis, three-color colocalization experiments were carried out to determine the spatial relationship among PRMPs, clathrin heavy chains, and membrane density in cultured adipocytes (Fig. 9). In these studies, PtdIns(4,5)P_2 is targeted with ECFP/PLCδ1-PH (blue regions in Fig. 9A). The plasma membrane is distinct from the endocytic membrane, as determined by extracellular Alx488-ConA labeling after cell fixation (green regions in Fig. 9B; see also discussion about Fig. 8). The cell was subsequently deter-

41 by 33 by 11 μm. O, origin. (C and D) Plots of EGFP (green line) and Alx594 (red line) fluorescence intensities for lines drawn across the two cells (C) and for lines drawn across the right-side cell (D). The arrow in panel D indicates an additional shoulder associated with the EGFP/PLCδ1-PH peak. (F) magnified colocalization image showing part of the PRMP on the right-side cell (red arrows in panels A, B, E, and F). It is a 1.5-μm cell section (yellow outline in panel E) that consisted of six *z* planes (i.e., *z*6 to *z*11) tilted 20° out of the paper. EGFP (green) and Alx594 (red) fluorescence images were rescaled between 30 and 90 and between 15 and 45, respectively, before being merged in the colocalization image. An 8-bit two-color intensity square (i.e., the color square in panel F; white indicates colocalized regions) was used. Thus, the colocalization image was prepared in such a way that most of the EGFP/PLCδ1-PH- or Alx594-ConA-labeled structures were visible but background noise was mostly eliminated to avoid being mistaken as intracellular structures. The blue arrow in panel F indicates the PtdIns(4,5)P_2-containing structures beneath the plasma membrane. The cells were serum starved for >2 h. Scale bars: panel B, 5 μm; panel F, 1 μm.

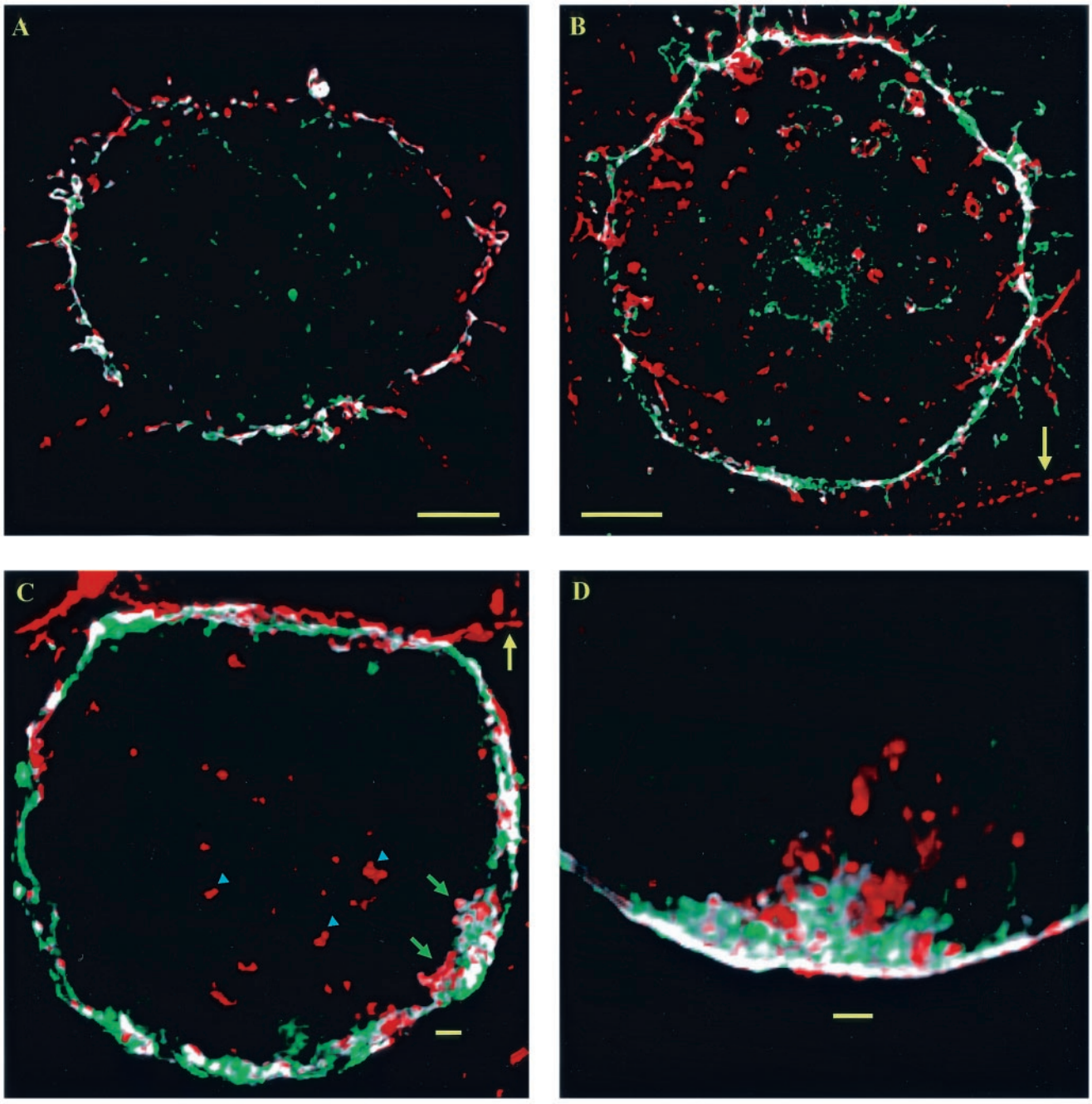

FIG. 8. PtdIns(4,5)P_2-containing vesicular structures beneath the plasma membrane are endocytic. Differential Alx594-ConA staining of adipocytes before (B to D) and after (A) formaldehyde fixation reveals the endocytic nature of the PtdIns(4,5)P_2-containing membranes. Living cells expressing EGFP/PLCδ1-PH were labeled with Alx594-ConA at 37°C (B to D). Colocalization images of deconvolved 3D structures (green, EGFP/PLCδ1-PH; red, Alx594-ConA; white, colocalized regions) were prepared as described in the legend to Fig. 7. (A and B) Sections (0.75 μm) of the bottom membranes attached to the coverslips, demonstrating differential Alx594-ConA staining before (B) and after (A) cell fixation. (C and D) Cross sections (0.75 and 1 μm, respectively) exposing endocytosis processes in two different adipocytes. Green arrows in panel C indicate endocytic vesicles containing both EGFP/PLCδ1-PH and Alx594-ConA and lining the inner leaflet of the plasma membrane. Cyan arrowheads in panel C indicate intracellular vesicles containing only Alx594-ConA. Yellow arrows in panels B and C indicate parts of neighboring cells labeled with Alx594-ConA only. Scale bars: A and B, 5 μm; C and D, 1 μm.

gent permeabilized, and clathrin heavy chains were immunofluorescently labeled with RhD-derivatized antibody (red regions in Fig. 9C). As expected, clathrin heavy chains concentrate in the perinuclear region and on the plasma membrane (Fig. 9C), where clathrin-assisted membrane trafficking predominantly occurs (43). As a result of detergent permeabilization, Alx488-ConA probe also leaks into the cell (Fig. 9B). Despite this complication, it is clear from examining the 3D projection

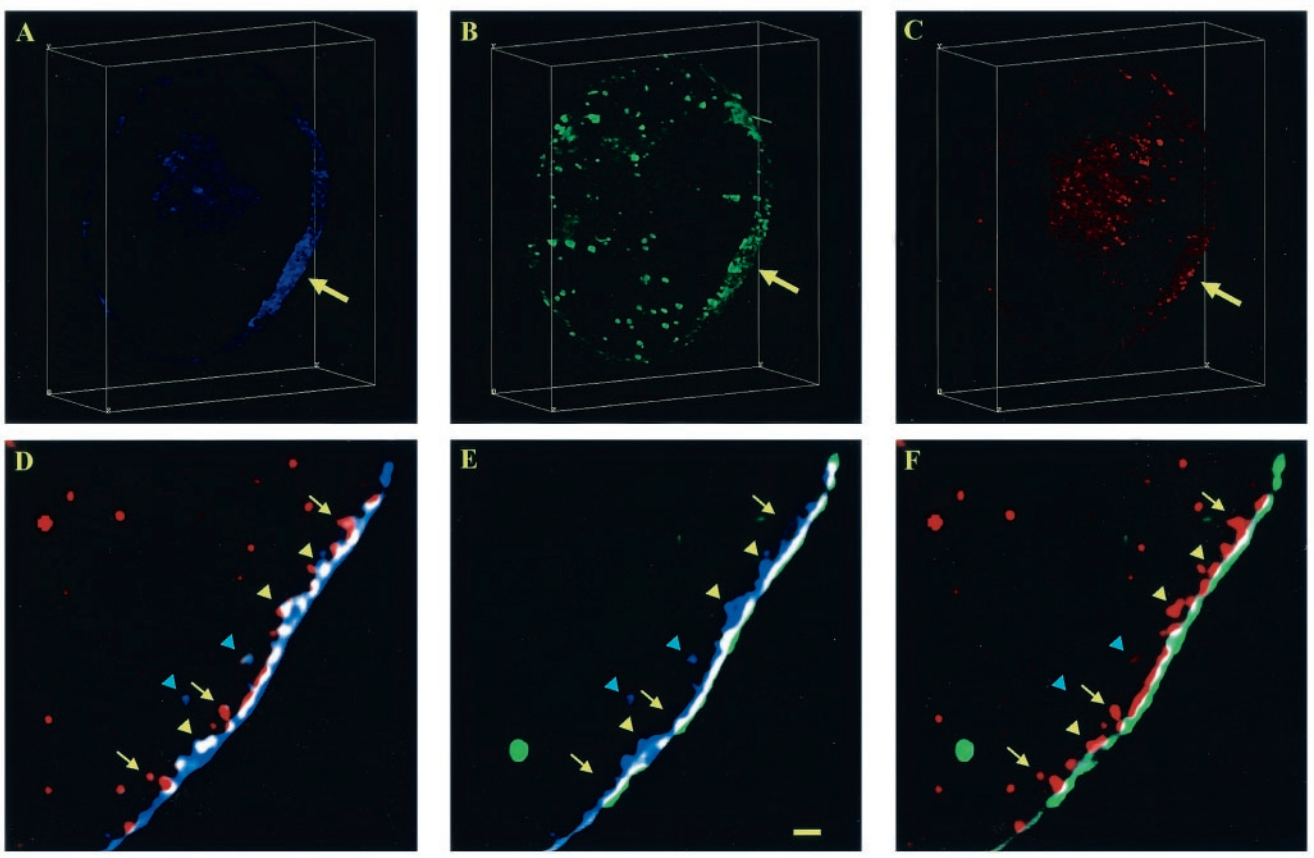

FIG. 9. PRMPs colocalize with active zones of clathrin-assisted endocytosis in cultured adipocytes. (A to C) The plasma membrane of an adipocyte transiently expressing ECFP/PLCδ1-PH (A, blue) was labeled with extracellular Alx488-ConA (B, green) after cell fixation, followed by cell permeabilization and immunofluorescence labeling (RhD-conjugated antibody) of clathrin heavy chains (C, red). Cross sections (5 μm) (i.e., *z*16 to *z*35) of the adipocyte were projected within 3D grids measuring 38 by 44 by 15 μm, exposing a PtdIns(4,5)P_2-rich (arrow in panel A) and lipid-dense (arrow in panel B) plasma membrane patch (i.e., PRMP) colocalizing with concentrated clathrin heavy chains (arrow in panel C). (See movie 7 at http://invitro.umassmed.edu/~sh/supplements/supplements.html for a complete set of colocalization images of the whole-cell section shown in panels A to C.) (D to F) Representative magnified, two-color colocalization images (Fig. 7) of a 0.5-μm cell section. Yellow and cyan arrowheads indicate colocalization of PtdIns(4,5)P_2 and clathrin heavy chains on and beneath the plasma membrane, respectively; yellow arrows indicate clathrin-coated vesicles emerging from the plasma membrane. All image stacks were acquired with the CFP, YFP, and RhD fluorescence channels without cross contamination (see Materials and Methods) and were deconvolved with a superresolution deconvolution algorithm. All images were visualized with 8-bit single-color intensity scales. The images in panels A to C were rescaled between 10 and 100, and the images in panels D to F were rescaled between 15 and 45. The cell was serum starved for >2 h and was subsequently insulin stimulated for 10 min at 37°C. Scale bar, 1 μm.

images that the PtdIns(4,5)P_2- and membrane-rich region (i.e., a PRMP) (arrows in Fig. 9A and B) also contains increased amounts of the clathrin subunit (arrow in Fig. 9C). Whether or not the cells are insulin stimulated (Fig. 9) or serum starved (data not shown), this spatial correlation between active regions of clathrin-assisted endocytosis and PRMPs are observed in all nine adipocytes examined by the three-color colocalization method. These results are consistent with the hypothesis that PtdIns(4,5)P_2 enrichment in PRMPs leads to enhanced PtdIns(4,5)P_2 interactions with the downstream effector molecules that assemble the clathrin coat (22, 43), thus focusing endocytic activities in active zones of the adipocyte surface membrane.

The detailed spatial relationships identified for the cellular structures by the three fluorescent labels are revealed upon examination of magnified colocalization images (sample *z* sections of 0.5 μm) (Fig. 9D to F). Figure 9D shows extensive colocalization (white regions) between clathrin heavy chains (red regions) and PtdIns(4,5)P_2-containing membranes (blue regions). Some PtdIns(4,5)P_2-containing structures are distinct from the plasma membrane, which is marked with extracellular Alx488-ConA labeling (green regions in Fig. 9E). Since clathrin-coated endocytotic vesicles originate from the inner leaflet of the plasma membrane, while Alx488-ConA labels the outer leaflet, there is only a partial overlap in anticlathrin and Alx488-ConA fluorescence (Fig. 9F), with these two signals being biased toward the interior and toward the exterior of the cell, respectively. Detailed examination of Fig. 9D to F further reveals PtdIns(4,5)P_2-containing and clathrin-coated "vesicles" emerging from the plasma membrane (yellow arrowheads). There are also nascent "vesicles" predominantly decorated with clathrin heavy chains and containing little or no PtdIns(4,5)P_2 (yellow arrows). Similarly, a few PtdIns(4,5)

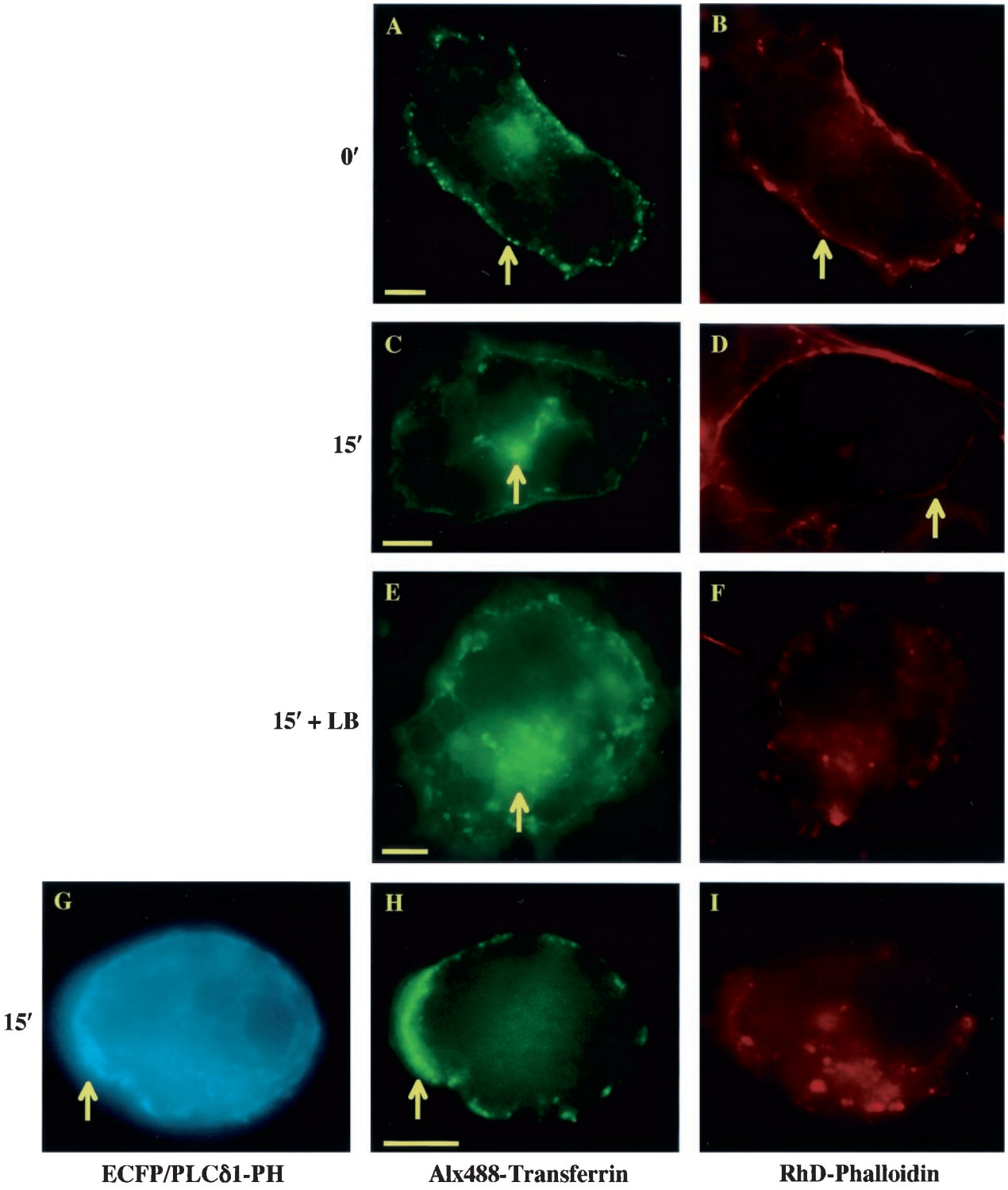

FIG. 10. Transferrin endocytosis in 3T3-L1 adipocytes. (A, C, E, and H) Differentiated adipocytes (day 5) expressing hTFRc were incubated with Alx488-TF for 1 h at 4°C to allow ligand-receptor binding on the plasma membrane (arrow in panel A). The cells were subsequently warmed to 37°C and incubated for 15 min to allow transferrin uptake (arrows in panels C and E). (B, D, F, and I) The cells were fixed in 4% formaldehyde and stained with Rhd-PhD for F-actin. Arrows in panels B and D indicate cortical F-actin, while actin filaments were disrupted by either LB treatment (F) or expression of ECFP/PLCδ1-PH (I). (G and H) Expression of the fusion protein (G) sequesters plasma membrane PtdIns(4,5)P_2 but does not interfere with Alx488-TF binding to its receptors on the cell surface (H). However, transferrin uptake in these cells is inhibited (H). In contrast, a majority of cells in which cortical F-actin is completely disrupted by LB treatment have normal transferrin endocytosis (E and F). Interestingly, transferrin labeling of the cell surface appears to be polarized [arrows in panels G and H indicate a membrane region enriched in PtdIns(4,5)P_2 and surface-bound transferrin]. Alx488 fluorescence in panel H was imaged in the YFP channel to avoid fluorescence from ECFP/PLCδ1-PH (see Materials and Methods). Scale bars, 5 μm.

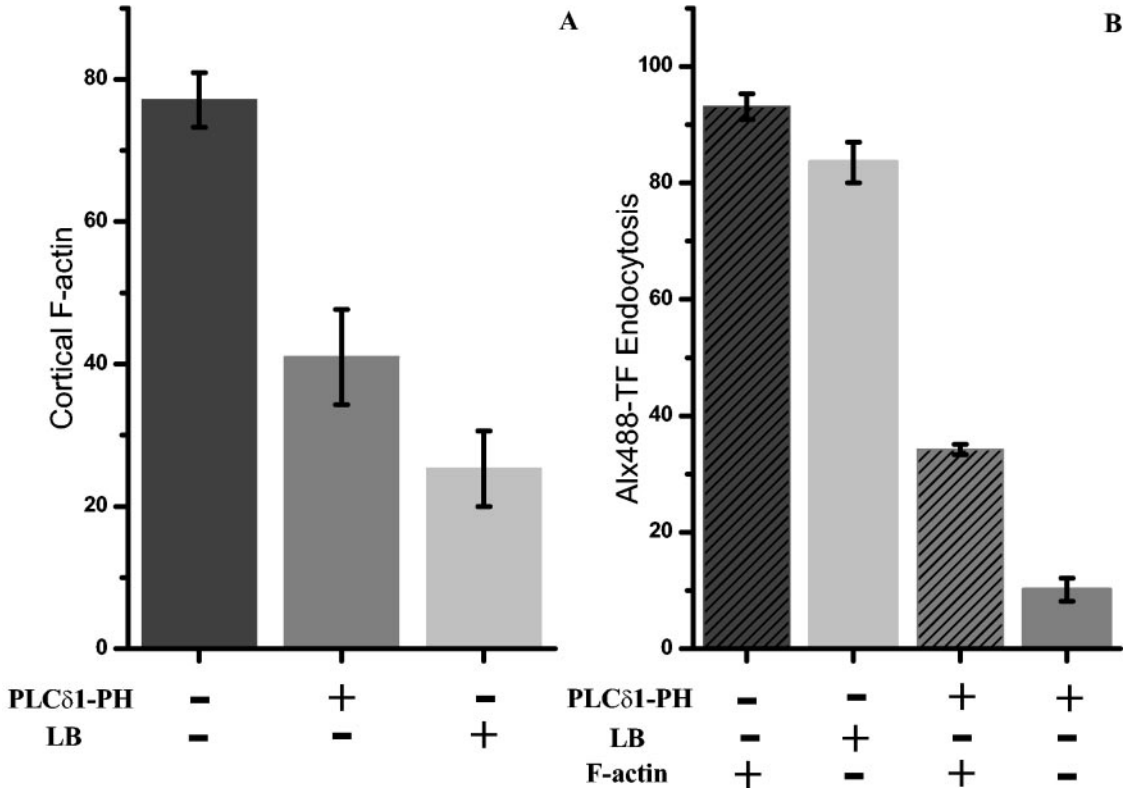

FIG. 11. Transferrin endocytosis is critically dependent on plasma membrane PtdIns(4,5)P_2 but is only modestly facilitated by the actin cytoskeleton. (A) Summary of cortical F-actin formation (i.e., F-actin positive) as a function of ECFP/PLCδ1-PH expression (i.e., PLCδ1-PH positive) or LB treatment. Cells in which a complete or a partial cortical actin cytoskeleton was preserved were counted as F actin positive. (B) Percentages of cells undergoing transferrin endocytosis as a function of plasma membrane PtdIns(4,5)P_2 (sequestered by ECFP/PLCδ1-PH) and/or F-actin (disrupted by LB treatment or ECFP/PLCδ1-PH expression). Error bars are standard errors of the mean from two independent experiments.

P_2-containing "vesicles" with residual clathrin labeling are found close to the plasma membrane (cyan arrowheads). Importantly, colocalization between clathrin heavy chains and PtdIns(4,5)P_2 in these images (Fig. 9D to F) occurs only in the vicinity of the plasma membrane. These observations provide direct evidence supporting the hypothesized PtdIns(4,5)P_2 turnover during clathrin-assisted endocytosis (22, 43). Slice-by-slice colocalization images of the PRMP shown in Fig. 9A to C are shown in movie 7 at http://invitro.umassmed.edu/~sh/supplements.html.

PtdIns(4,5)P_2 but not F actin is critically important for transferrin endocytosis. The concomitant enrichment of PtdIns(4,5)P_2 and cortical F actin within and beneath PRMPs, respectively (Fig. 2 to 5), suggests that both may play roles in clathrin-assisted endocytosis. Since receptor-mediated transferrin uptake is a classic example of clathrin-assisted endocytosis, this process was investigated in 3T3-L1 adipocytes as a function of PtdIns(4,5)P_2 availability and actin polymerization (Fig. 10 and 11). Differentiated adipocytes expressing hTFRc were incubated with Alx488-conjugated transferrin at 4°C to allow ligand-receptor binding on the plasma membrane (arrow in Fig. 10A). The cells were subsequently warmed to 37°C and incubated for 15 min to facilitate transferrin uptake (arrows in Fig. 10C and E). Some of these cells also highly express ECFP/PLC δ1-PH (Fig. 10G), which sequesters PtdIns(4,5)P_2 in the plasma membrane and in some cases completely prevents cortical F-actin formation (Fig. 5G to I and 10G to I). Alternatively, F-actin was disrupted by LB treatment (Fig. 10E and F). As visualized by RhD-PhD staining, 77% ± 4% of the hTFRc-expressing adipocytes have cortical F-actin (Fig. 11A) (35). This percentage decreases to 41% ± 6.7% for cells expressing EGFP/PLC δ1-PH and to 25% ± 5% for LB-treated cells (Fig. 11A). For cells that have cortical F-actin, 93% ± 2% show clear transferrin endocytosis after 15 min (Fig. 10C and D). This percentage decreases to 34% ± 1% for cells expressing EGFP/PLC δ1-PH but retaining cortical F-actin (Fig. 11B). For cells expressing the fusion protein and completely lacking F-actin, only 10% ± 2% undergo transferrin endocytosis. This further inhibition in transferrin endocytosis (i.e., from 34% ± 1% to 10% ± 2%) in EGFP/PLC δ1-PH expressing cells is only partially attributed to the loss of the cortical cytoskeleton, since disruption of F-actin with LB causes only a slight decrease in the rate of transferrin uptake (i.e., from 93% ± 2% to 84% ± 4%) (Fig. 11B). Rather, in cells that lack cortical F-actin due to high-level EGFP/PLCδ1-PH expression, PtdIns(4,5)P_2 in the plasma membrane likely is sequestered to a higher degree and therefore is more effective in inhibiting transferrin endocytosis than cortical F-actin. Thus, it appears that clathrin-assisted endocytosis is critically dependent on the

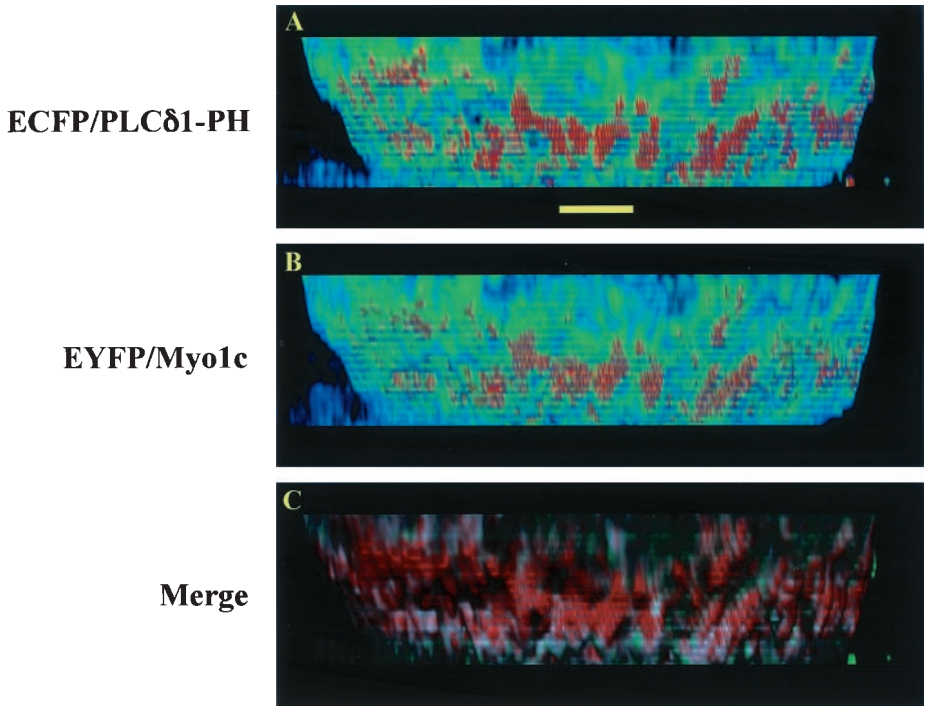

FIG. 12. PRMPs concentrate the actin-binding motor protein Myo1c beneath the plasma membrane. (A and B) High-magnification image stacks consisting of 55 *z* sections (i.e., 13.75 μm) were acquired for a fixed adipocyte coexpressing ECFP/PLCδ1-PH and EYFP/Myo1c with the CFP and YFP fluorescence channels without cross talk (see Materials and Methods). After the image stacks were processed with a superresolution deconvolution algorithm, surface distribution patterns for PtdIns(4,5)P_2 (A) and Myo1c (B), visualized with 8-bit false-color intensity scales (rescaled at between 10 and 100) (Fig. 1), show perfect colocalization on side views of the plasma membrane. (C) The colocalization image (red, ECFP/PLCδ1-PH; green, EYFP/Myo1c; white, colocalized regions), visualized with 8-bit single-color intensity scales (rescaled at between 10 and 100), shows that Myo1c fluorescence originates predominantly beneath the inner leaflet of the plasma membrane labeled with ECFP/PLCδ1-PH. The adipocyte was serum starved for >2 h and was subsequently insulin stimulated for 30 min at 37°C. Scale bar, 5 μm.

availability of PtdIns(4,5)P_2 in the plasma membrane but is only partially facilitated by the cortical F-actin cytoskeleton.

PRMPs appear to direct Myo1c-induced membrane ruffling near the substratum. Based on data showing that cortical actin filaments are concentrated beneath PRMPs in cultured adipocytes (Fig. 5), we tested whether actin-based functions may be similarly localized at PRMP sites. One actin-based cellular process is plasma membrane ruffling (27, 45), which has been reported to be intensified by insulin stimulation in 3T3-L1 adipocytes (33, 35). However, ruffling events occur mainly at the adherent membrane of adipocytes in cultures (35) and are fairly infrequent. However, the frequency and size of plasma membrane ruffles in cultured adipocytes can be amplified by the expression of unconventional Myo1c (5). We therefore first evaluated the distribution of expressed Myo1c in 3T3-L1 adipocytes. Figure 12 shows that a representative adipocyte transiently expressing both ECFP/PLCδ1-PH (Fig. 12A) and a fusion protein linking EYFP to Myo1c (EYFP/Myo1c) (Fig. 12B) displays PRMPs colocalized exclusively with regions of concentrated EYFP/Myo1c. Furthermore, in the colocalization image (Fig. 12C; red regions indicate ECFP/PLC δ1-PH, green regions indicate EYFP/Myo1c, and white regions indicate colocalization), EYFP/Myo1c fluorescence is localized mostly beneath the inner leaflet of the plasma membrane labeled with ECFP/PLCδ1-PH. Thus, EYFP/Myo1c is concentrated at regions of dense F-actin, which are also exclusively localized at PRMPs (Fig. 5). These findings are consistent with electron microscopic images showing that Myo1c is localized mostly at the cortical F-actin network beneath the plasma membrane of cultured adipocytes (4).

In live cells, the overexpression of Myo1c leads to dramatic ruffling events near the substratum (Fig. 13; see also movie 8 at http://invitro.umassmed.edu/~sh/supplements/supplements.html) (5). Large membrane ruffles have also been observed, albeit at a much lower frequency, in normal adipocytes (yellow arrows in Fig. 1D). The fact that these ruffles occur predominantly in membranes close to the coverslip (Fig. 1D and 13; see also movie 8 at http://invitro.umassmed.edu/~sh/supplements/supplements.html) is consistent with current hypotheses on actin-based cellular motility (45). Thus, a membrane protrusion occurring at the bottom of a cell, possibly driven by concentrated Myo1c activity on F-actin, can briefly attach to the coverslip. Since the immobile adipocyte does not retract on the opposite end of this protrusion event, this temporary attachment cannot be sustained. Therefore, the membrane protrusion eventually detaches and peels back, resulting in a classic ruffling event (see movie 8 at http://invitro.umassmed.edu/~sh/supplements/supplements.html). In contrast, there are no physical structures for membrane attachment in the spaces above the coverslip, and large-scale membrane ruffles are seldom observed in these regions in our studies. Importantly, PRMPs are found immediately above the Myo1c-induced membrane ruffles (labeled 1 to 3 in Fig. 13A), and little large-scale ruffling occurs in regions not associated with PRMPs.

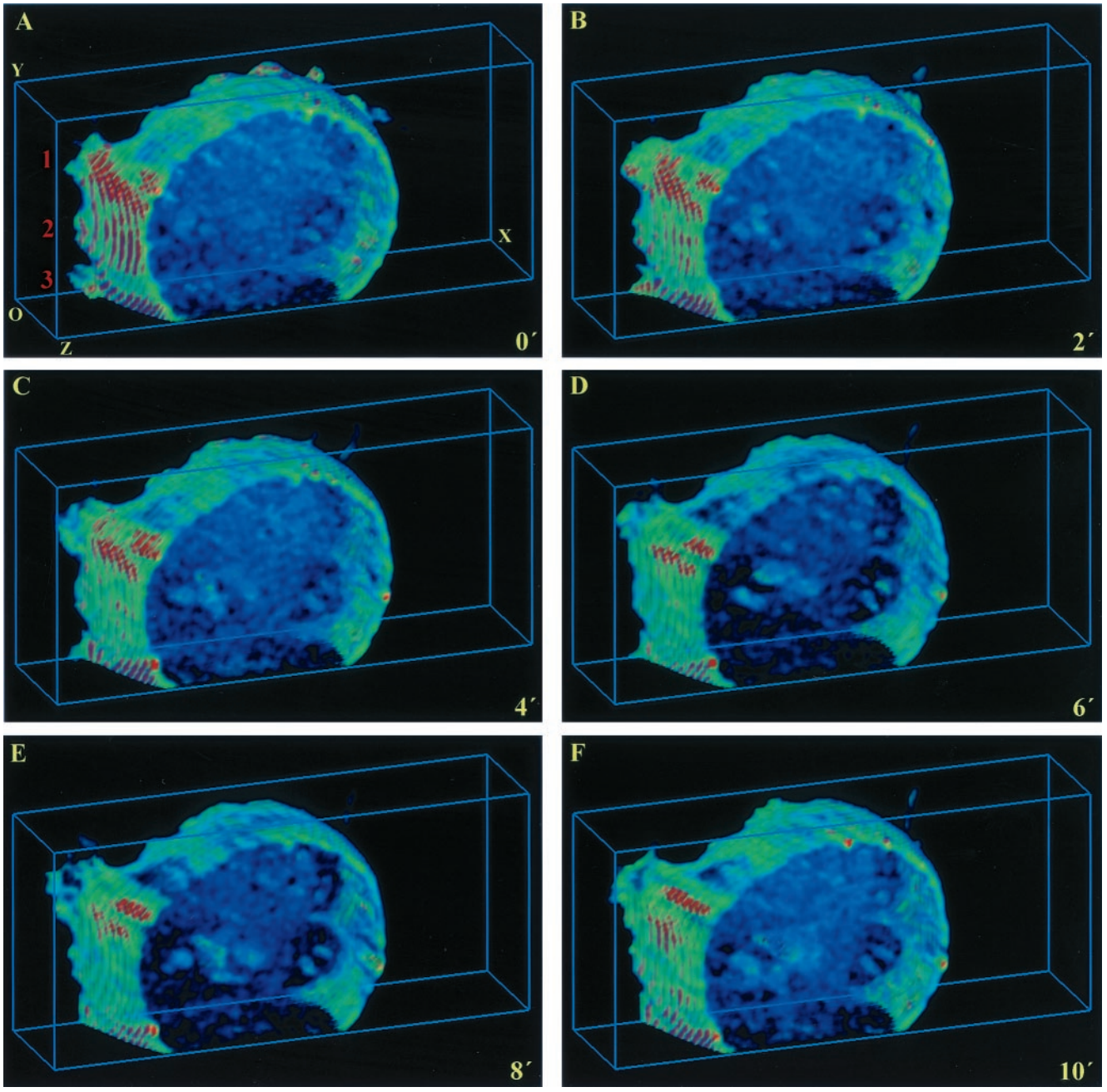

FIG. 13. PRMPs spatially correlate with Myo1c-induced membrane ruffles. Ultrafast-acquisition deconvolution microscopy was carried out every 30 s for 10 min for a living adipocyte expressing both ECFP/PLCδ1-PH and EYFP/Myo1c fusions. The CFP fluorescence was excited with the 458-nm laser line of an Ar laser. Therefore, there is significant fluorescence bleedthrough from the CFP channel to the YFP channel, while reverse bleedthrough is negligible. Therefore, only the CFP fluorescence images depicting PtdIns(4,5)P_2 distribution and dynamics are shown, with the understanding that major membrane ruffles (labeled 1 to 3 in panel A) are caused by Myo1c overexpression (see Results). Deconvolved images were projected within 3D grids measuring 18 by 42 by 10 μm and were visualized with 8-bit false-color intensity scales (rescaled at between 10 and 100). Representative images at 0, 2, 4, 6, 8, and 10 min are shown. O, origin. (See movie 8 at http://invitro.umassmed.edu/~sh/supplements/supplements.html for the complete image sequence.)

Detailed examination of movie 8 at http://invitro.umassmed.edu/~sh/supplements/supplements.html reveals that the PRMP above the most active ruffle (ruffle 1) persists throughout the experiment, while the one above the least active ruffle (ruffle 2) diminishes (Fig. 13). Significantly, all PRMPs regroup somewhat at these same membrane sites toward the end of the experiment (Fig. 13F), suggesting a localized mechanism coordinating PtdIns(4,5)P_2 concentration in the plasma membrane, F-actin dynamics, and Myo1c-driven membrane trafficking at these specialized membrane patches.

DISCUSSION

An important conclusion derived from the present findings is that plasma membranes of cultured adipocytes are complex and heterogeneous structures that contain organized zones of high actin polymerization, endocytic, and membrane-ruffling activities. Using advanced imaging techniques, we found that both lipid and protein constituents of the plasma membrane are distributed nonuniformly in 3D space. This distribution has the significant consequence of concentrating the signaling molecule PtdIns(4,5)P_2 in micrometer-sized plasma membrane patches (i.e., PRMPs) (Fig. 1 to 5, 7 to 9, 12, and 13). Such preferential concentration of PtdIns(4,5)P_2 in specific regions of adipocyte surface membranes likely enhances PtdIns(4,5)P_2 interactions with downstream effectors [e.g., PtdIns(4,5)P_2-binding components of protein complexes that regulate actin polymerization and endocytosis]. Indeed, PRMPs are involved in the spatial organization of cortical F-actin (Fig. 5) and colocalize with active zones of endocytosis (Fig. 7 to 9). PRMPs display little movement on the cell surface of cultured adipocytes (see movie 4 at http://invitro.umassmed.edu/~sh/supplements/supplements.html). However, in adipocytes whose motility is dramatically enhanced by the expression of Myo1c, PRMPs show profound spatial correlation with Myo1c-induced membranes ruffles (Fig. 12 and 13; see also movie 8 at http://invitro.umassmed.edu/~sh/supplements/supplements.html). Thus, the imaging data presented here support the hypothesis that PRMPs constitute the major structural basis upon which multiple PtdIns(4,5)P_2-directed cellular activities take place. Interestingly, insulin stimulation does not seem to alter the global organization of PRMPs (see movie 4 at http://invitro.umassmed.edu/~sh/supplements/supplements.html).

The fusion protein EGFP/PLCδ1-PH has been demonstrated in many laboratories to be a sensitive indicator of PtdIns(4,5)P_2 in multiple cell types (2, 3, 44). In agreement with previous observations (48, 56, 67), PtdIns(4,5)P_2 is found primarily in the plasma membrane of cultured 3T3-L1 adipocytes. EGFP/PLCδ1-PH affinity toward PtdIns(4,5)P_2 is relatively weak (K_d, ~2 μM) (39), and the plasma membrane-bound fusion protein undergoes rapid (~1 s) equilibrium with its cytosolic counterpart (64). Therefore, EGFP/PLCδ1-PH is specifically targeted to plasma membrane PtdIns(4,5)P_2 but is unlikely to induce lateral PtdIns(4,5)P_2 segregation in micrometer-sized membrane domains (44). Furthermore, a major mechanism contributing to PRMP formation is local membrane folding concentrating PtdIns(4,5)P_2 in 3D space (Fig. 2 to 4). Such an uneven distribution of plasma membrane content is intrinsically present on the adipocyte surface, as evidenced by 3D images (see movie 6 at http://invitro.umassmed.edu/~sh/supplements/supplements.html) of live cells labeled only with Alx594-ConA. Therefore, PRMPs are not the result of EGFP/PLCδ 1-PH expression or the electroporation process introducing plasmid DNA. On the other hand, EGFP/PLCδ1-PH is not very useful for visualizing PtdIns(4,5)P_2 in intracellular membranes because intracellular PtdIns(4,5)P_2 is difficult to image against the background fluorescence of EGFP/PLCδ1-PH solubilized in the cytosol or bound to Ins(1,4,5)P_3. In fact, quantitative electron microscopic results have shown that the level of EGFP/PLCδ1-PH expressed in the cytoplasm is higher than those in intracellular membranes but significantly lower than that on the plasma membrane (68). Nevertheless, under favorable expression and imaging conditions, we observed some EGFP/PLCδ1-PH localization in the perinuclear region of adipocytes (data not shown), where the fusion protein presumably binds to PtdIns(4,5)P_2 in Golgi membranes (23, 34).

Heterogeneous segregation of PtdIns(4,5)P_2 in plasma membranes was previously reported based on single-plane, wide-field, or confocal microscopy (38, 59, 66). However, the full extent of PtdIns(4,5)P_2 spatial organization is revealed in the present studies by use of a custom-built, laser-illuminated, ultrafast-acquisition deconvolution microscope. This technique allowed us to acquire 3D images within a time frame (~1 s) that is virtually insensitive to cell movements and with minimal interference from photobleaching (51). During the course of our studies, a report of PtdIns(4,5)P_2-rich membrane domains in another cell type surprisingly suggested that they may result entirely from local membrane folds unresolved by fluorescence microscopy (66). This hypothesis is supported by our observation that PRMPs in adipocytes colocalize with membrane-dense domains labeled with BODIPY-HPC or Alx594-ConA (Fig. 2 to 4). The existence of such PRMPs is consistent with electron microscopic images showing numerous small (i.e., 25 to 150 nm) invaginations and vesicles in and near the surface membranes of rat adipocytes (12, 61). Remarkably, clusters of these suboptical-resolution structures organize into large patches that are apparent on the adipocyte surface under fluorescence microscopic observation (61). These membrane invaginations significantly increase the total surface area of an adipocyte cell and may reflect adaptive specialization of the plasma membrane to handle a massive membrane trafficking volume occurring in this particular cell type (61). Furthermore, quantitative, ratiometric image analysis carried out in the present studies indicates that PtdIns(4,5)P_2 is also laterally concentrated in PRMPs (Fig. 3 and 4). These data agree with previous results obtained from quantitative fluorescence and electron microscopic studies demonstrating PtdIns(4,5)P_2 enrichment in the membranes of phagosomal cups and lamellipodia, respectively (6, 68). On the basis of earlier data and our present results, the mechanisms of increased membrane content and increased lateral PtdIns(4,5)P_2 concentration both appear to contribute to the formation of PRMPs.

Regardless of the specific mechanism for concentrating PtdIns(4,5)P_2 in PRMPs, we found that these plasma membrane structures are effective in concentrating PtdIns(4,5)P_2-directed actin polymerization (Fig. 5) and endocytic (Fig. 7 to 9) activities in segregated regions on the adipocyte surface. The importance of PtdIns(4,5)P_2 in managing F-actin assembly and remodeling has been well documented (10, 32, 54, 58). We found that PRMPs are exclusively associated with regions of dense cortical F actin (Fig. 5). This direct correlation between the spatial concentrations of PtdIns(4,5)P_2 and F-actin is consistent with atomic force microscopic measurements, which demonstrated that the adhesion forces between the plasma membrane and its underlying F-actin cytoskeleton were directly proportional to PtdIns(4,5)P_2 levels in the membrane (50). In addition, we find that sequestration of PtdIns(4,5)P_2 in the plasma membrane by the overexpression of EGFP/PLCδ1-PH inhibits cortical F-actin formation (Fig. 5G to I, 10G to I, and 11A). These results indicate that PRMPs play a

role in the spatial organization of the actin cytoskeleton. In contrast, the disruption of cortical F-actin by LB does not interfere with PtdIns(4,5)P_2 production or PRMP formation (Fig. 6; see also movie 5 at http://invitro.umassmed.edu/~sh/supplements/supplements.html). It appears that the uneven distribution of plasma membrane content, a major mechanism contributing to PRMP formation (Fig. 2 to 4), is an intrinsic property of animal cells (24). Through the use of various techniques and cell types, it has been estimated that 40 to 1,000% excess membrane is stored in membrane folds, microvilli, and caveolae (17, 19, 52, 55, 61, 72, 73). Many mechanisms could contribute to such complexity in the 3D organization of the plasma membrane; these include lipid compositions (8, 29), membrane-protein interactions (20, 44), and cytoskeletal elements (spectrin-ankyrin network, F-actin, microtubules, intermediate filaments, and so forth) (24, 31). These mechanisms cannot be completely abolished by the disruption of F actin alone (see movie 5 at http://invitro.umassmed.edu/~sh/supplements/supplements.html), consistent with the fact that adipocytes completely lacking cortical F actin still maintain a distinct irregular cellular morphology characteristic of fully differentiated adipocytes (see movie 5 at http://invitro.umassmed.edu/~sh/supplements/supplements.html).

Increasing evidence indicates that PtdIns(4,5)P_2 functions in highly localized membrane structures to regulate cellular processes (14, 15, 32, 43, 44, 48). Studies on large-scale membrane dynamics associated with phagocytosis and bacterial invasion have demonstrated that transient, focal PtdIns(4,5)P_2 accumulation is essential for developing membrane protrusions surrounding the invading particles. Interestingly, in those previous studies, the complete loss of PtdIns(4,5)P_2 on internalized membranes coincided with membrane fission (6, 60). Consistent with these findings, our results obtained with superresolution deconvolution microscopy reveal PtdIns(4,5)P_2-containing, submicrometer-sized vesicular structures immediately beneath PRMPs (Fig. 7). PtdIns(4,5)P_2 is subsequently eliminated from such "vesicles" maturing toward the interior of the cell (Fig. 8C and D). These observations suggest that PtdIns(4,5)P_2 dynamics associated with phagocytosis and bacterial invasion may also occur on smaller spatial scales and are associated with clathrin-assisted endocytosis (15, 43). Clathrin coat assembly on budding endosomes is thought to depend on the local presence of PtdIns(4,5)P_2, while PtdIns(4,5)P_2 hydrolysis precedes clathrin coat disassembly and probably also endosome fission (15, 22). This hypothesis is directly supported by the images shown in Fig. 9. In a membrane region associated with active endocytosis, budding "vesicles" containing both clathrin heavy chains and PtdIns(4,5)P_2 are found to emerge from the inner leaflet of the plasma membrane (Fig. 9D to F; see also movie 7 at http://invitro.umassmed.edu/~sh/supplements/supplements.html). Most significantly, a PMRP completely colocalizes with this active region of endocytosis (Fig. 9A to C), consistent with the observation that plasma membrane PtdIns(4,5)P_2 is critically important for transferrin uptake, a classic example of clathrin-assisted endocytosis (Fig. 10 and 11). Taken together, the data suggest a mechanism for spatially focusing PtdIns(4,5)P_2 signaling to clathrin-mediated endocytosis at specific regions of the cell surface through the formation of PRMPs. In contrast, completely abolishing cortical F-actin with LB treatment only modestly inhibits transferrin uptake, a finding which adds to a large body of conflicting evidence relating to the exact function of F actin in the endocytosis process (18, 21, 49).

The correlations between the spatial dispositions of PRMPs in the adipocyte plasma membrane and similarly localized zones of concentrated F-actin and high endocytic activities do not provide conclusive evidence that there is a causative link between them. It could be argued that more endocytosis occurs at PRMPs simply due to the larger amounts of membranes present at these regions to be internalized. In order to further investigate the issue of the functionality of PRMPs, we used a protein, the molecular motor Myo1c, which is known to require F-actin for its actions (4). As expected, expressed Myo1c localized predominantly at regions of high cortical F-actin levels that occur just beneath PRMPs (Fig. 12). Significantly, the membrane ruffling that is mediated by Myo1c in these adipocytes occurs predominantly at substratum locations marked by PRMPs (Fig. 13; see also movie 8 at http://invitro.umassmed.edu/~sh/supplements/supplements.html) (5). In other words, Myo1c apparently can function efficiently to cause large membrane ruffles only at sites on the plasma membrane where it is concentrated by large amounts of F-actin, beneath PRMPs. These data indicate that a function of PRMPs is to localize membrane-ruffling events, presumably by concentrating F actin and Myo1c to enhance their promotion of ruffling. Little or no membrane ruffling occurs away from PRMPs in the adipocyte plasma membrane. These considerations provide strong support for the hypothesis that PRMPs have important functions in directing cellular processes in adipocytes. The fact that Myo1c also promotes GLUT4 translocation in response to insulin (4) suggests that PRMPs may also promote this process. Future experiments are directed toward testing this possibility.

ACKNOWLEDGMENTS

We thank Joseph Virbasius and Darcy Pomerleau for providing the ECFP/PLCδ1-PH construct and My Chouinard for preparing 3T3-L1 adipocytes. Thoughtful discussions with Silvia Corvera and David Lambright aided in the completion of this article.

This work was supported by National Institutes of Health program project grant DK60564.

REFERENCES

1. **Arbuzova, A., A. A. P. Schmitz, and G. Vergeres.** 2002. Cross-talk unfolded: MARCKS proteins. Biochem. J. **2002:**1–12.
2. **Bajno, L., and S. Grinstein.** 1999. Fluorescent proteins: powerful tools in phagocyte biology. J. Immunol. Methods **232:**67–75.
3. **Balla, T., and P. Varnai.** 2002. Visualizing cellular phosphoinositide pools with GFP-fused protein-modules. Sci. STKE **2002:**PL3.
4. **Bose, A., A. Guiherme, S. I. Robida, S. M. C. Nicoloro, Q. L. Zhou, Z. Y. Jiang, D. P. Oomerleau, and M. P. Czech.** 2002. Glucose transporter recycling in response to insulin is facilitated by myosin Myo1c. Nature **420:**821–824.
5. **Bose, A., S. Robida, P. S. Furcinitti, A. Chawla, K. Fogarty, S. Corvera, and M. P. Czech.** 2004. Unconventional myosin Myo1c promotes membrane fusion in a regulated exocytic pathway. Mol. Cell. Biol. **24:**5447–5458.
6. **Botelho, R. J., M. Teruel, R. Dierckman, R. Anderson, A. Wells, J. D. York, T. Meyer, and S. Grinstein.** 2000. Localized biphasic changes in phosphatidylinositol-4,5-bisphosphate at sites of phagocytosis. J. Cell Biol. **151:**1353–1368.
7. **Brown, F. D., A. L. Rozelle, H. L. Yin, T. Balla, and J. G. Donaldson.** 2001. Phosphatidylinositol 4,5-bisphosphate and Arf6-regulated membrane traffic. J. Cell Biol. **154:**1007–1017.
8. **Brown, W., K. Chambers, and A. Doody.** 2003. Phospholipase A2 (PLA2) enzymes in membrane trafficking: mediators of membrane shape and function. Traffic **4:**214–221.
9. **Cantley, L. C., K. R. Auger, C. Carpenter, B. Duckworth, A. Graziani, R. Kapeller, and S. Soltoff.** 1991. Oncogenes and signal transduction. Cell **64:**281–302.

10. **Caroni, P.** 2001. Actin cytoskeleton regulation through modulation of PI(4,5)P_2 rafts. EMBO J. **20:**4332–4336.
11. **Carrington, W. A., R. M. Lynch, E. D. Moore, G. Isenberg, K. E. Fogarty, and F. S. Fay.** 1995. Superresolution three-dimensional images of fluorescence in cells with minimal light exposure. Science **268:**1483–1487.
12. **Chlapowski, F. J., B. K. Bertrand, J. Pessin, Y. Oka, and M. P. Czech.** 1983. The relationship of microvesicles to the plasmalemma of rat adipocytes. Eur. J. Cell Biol. **32:**24–30.
13. **Colarusso, P., and K. R. Spring.** 2002. Reticulated lipid probe fluorescence reveals MDCK cell apical membrane topography. Biophys. J. **82:**752–761.
14. **Cremona, O., and P. de Camilli.** 2001. Phosphoinositides in membrane traffic at the synapse. J. Cell Sci. **114:**1041–1052.
15. **Czech, M. P.** 2003. Dynamics of phosphoinositides in membrane retrieval and insertion. Annu. Rev. Physiol. **65:**791–815.
16. **Czech, M. P.** 2000. PIP2 and PIP3: complex roles at the cell surface. Cell **100:**603–606.
17. **Dulhunty, A. F., and C. Franzini-Armstrong.** 1975. The relative contributions of the folds and caveolae to the surface membrane of frog skeletal muscle fibers at different sacromere lengths. J. Physiol. (London) **250:**513–539.
18. **Ellis, S., and H. Mellor.** 2000. Regulation of endocytic traffic by Rho family GTPases. Trends Cell Biol. **10:**85–88.
19. **Evans, E.** 1992. Composite membranes and structured interfaces: from simple to complex designs in biology, p. 81–101. *In* B. P. Gaber and K. R. K. Easwaran (ed.), Biomembranes structure and function—the state of art. Adenine, New York, N.Y.
20. **Farsad, K., and P. De Camilli.** 2003. Mechanisms of membrane deformation. Curr. Opin. Cell Biol. **15:**372–381.
21. **Geli, M. I., and H. Riezman.** 1998. Endocytic internalization in yeast and animal cells: similar and different. J. Cell Sci. **111:**1031–1037.
22. **Gillooly, D. J., and H. Stenmark.** 2001. A lipid oils the endocytosis machine. Science **291:**993–994.
23. **Godi, A., P. Pertile, R. Meyers, P. Marra, G. Di Tullio, C. Lurisci, A. Luini, D. Corda, and M. A. De Matteis.** 1999. ARF mediates recruitment of PrdIns-4-OH kinase-β and stimulates synthesis of PtdIns(4,5)P_2 on the Golgi complex. Nat. Cell Biol. **1:**280–287.
24. **Hamill, O. P., and B. Martinac.** 2001. Molecular basis of mechanotransduction in living cells. Physiol. Rev. **81:**685–740.
25. **Hilgemann, D. W., S. Feng, and C. Nasuhoglu.** 2001. The complex and intriguing lives of PIP_2 with ion channels and transporters. Sci. STKE **2001:** RE19.
26. **Hinchliffe, K.** 2000. Intracellular signalling: is PIP_2 a messenger too? Curr. Biol. **10:**R104–R105.
27. **Honda, A., M. Nogami, T. Yokozeki, M. Yamazaki, H. Nakamura, H. Watanabe, K. Kawamoto, K. Nakayama, A. J. Morris, M. A. Frohman, and Y. Kanaho.** 1999. Phosphatidylinositol 4-phosphate 5-kinase alpha is a downstream effecter of the small G protein ARF6 in membrane ruffle formation. Cell **99:**521–532.
28. **Hope, H. R., and L. J. Pike.** 1996. Phosphoinositides and phosphoinositide-utilizing enzymes in detergent-insoluble lipid domains. Mol. Biol. Cell **7:**843–851.
29. **Huttner, W., and J. Zimmerberg.** 2001. Implications of lipid microdomains for membrane curvature, budding and fission. Curr. Opin. Cell Biol. **13:**478–484.
30. **Jacobson, K., and C. Dietrich.** 1999. Looking at lipid rafts? Trends Cell Biol. **9:**87–91.
31. **Janmey, P. A.** 1998. The cytoskeleton and cell signaling: component localization and mechanical couple. Physiol. Rev. **78:**763–781.
32. **Janmey, P. A., W. Xian, and L. A. Flanagan.** 1999. Controlling cytoskeleton structure by phosphoinositide-protein interactions: phosphoinositide binding protein domains and effects of lipid packing. Chem. Phys. Lipids **101:**93–107.
33. **Jiang, Z. Y., A. Chawla, A. Bose, M. Way, and M. P. Czech.** 2002. A phosphatidylinositol 3-kinase-independent insulin signaling pathway to N-WASP/Arp2/3/F-actin required for GLUT4 glucose transporter recycling. J. Biol. Chem. **277:**509–515.
34. **Jones, D. H., J. B. Morris, C. P. Morgan, H. Kondo, R. F. Irvine, and S. Cockcroft.** 2000. Type I phosphatidylinositol 4-phosphate 5-kinase directly interacts with ADP-ribosylation factor 1 and is responsible for phosphatidylinositol 4,5-bisphosphate synthesis in the Golgi compartment. J. Biol. Chem. **275:**13962–13966.
35. **Kanzaki, M., and J. E. Pessin.** 2001. Insulin-stimulated GluT4 translocation in adipocytes is dependent upon cortical actin remodeling. J. Biol. Chem. **276:**42436–42444.
36. **Kirov, S. A., and K. M. Harris.** 1999. Dendrites are more spiny on mature hippocampal neurons when synapses are inactivated. Nat. Neurosci. **2:**878–883.
37. **Korlach, J., P. Schwille, W. W. Watt, and G. W. Feigenson.** 1999. Characterization of lipid bilayer phases by confocal microscopy and fluorescence correlation spectroscopy. Proc. Natl. Acad. Sci. USA **96:**8461–8466.
38. **Laux, T., K. Fukami, M. Thelen, T. Golub, D. Frey, and P. Caroni.** 2000. GAP43, MARCKS, and CAP23 modulate PI(4,5)P_2 at plasmalemmal rafts, and regulate cell cortex actin dynamics through a common mechanism. J. Cell Biol. **149:**1455–1472.
39. **Lemmon, M. A., K. M. Ferguson, R. O'Brien, P. B. Sigler, and J. Schlessinger.** 1995. Specific and high-affinity binding of inositol phosphates to an isolated pleckstrin homology domain. Proc. Natl. Acad. Sci. USA **92:**10472–10476.
40. **Lifshitz, L. M., J. Collins, E. Moore, and J. Gauch.** 1994. Computer vision and graphics in fluorescence microscopy, p. 166–175. *In* Proceedings of the IEEE Workshop on Biomedical Image Analysis. IEEE Computer Society Press, Los Alamitos, Calif.
41. **London, E.** 2002. Insights into lipid raft structure and formation from experiments in model membranes. Curr. Opin. Struct. Biol. **12:**480–486.
42. **Marshall, J. G., J. W. Booth, V. Stambolic, T. Mak, T. Balla, A. D. Schreiber, T. Meyer, and S. Grinstein.** 2001. Restricted accumulation of phosphatidylinositol 3-kinase products in a plasmalemmal subdomain during Fc gamma receptor-mediated phagocytosis. J. Cell Biol. **153:**1369–1380.
43. **Martin, T. F.** 2001. PI(4,5)P_2 regulation of surface membrane traffic. Curr. Opin. Cell Biol. **13:**493–499.
44. **McLaughlin, S., J. Wang, A. Gambhir, and D. Murray.** 2002. PIP_2 and proteins: interactions, organization, and information flow. Annu. Rev. Biophys. Biomol. Struct. **31:**151–175.
45. **Mitchison, T. J., and L. P. Cramer.** 1996. Actin-based cell motility and cell locomotion. Cell **84:**371–379.
46. **Parton, R. G., J. C. Molero, M. Floetenmeyer, K. M. Green, and D. E. James.** 2002. Characterization of a distinct plasma membrane macrodomain in differentiated adipocytes. J. Biol. Chem. **277:**46769–46778.
47. **Patki, V., J. Buxton, A. Chawla, L. Lifshitz, K. Fogarty, W. Carrington, R. Tuft, and S. Corvera.** 2001. Insulin action on GLUT4 traffic visualized in single 3T3-L1 adipocytes using ultra-fast microscopy. Mol. Biol. Cell **12:**129–141.
48. **Payrastre, B., K. Missy, S. Giuriato, S. Bodin, M. Plantavid, and M. Gratacap.** 2001. Phosphoinositides: key players in cell signalling, in time and space. Cell. Signal. **13:**377–387.
49. **Qualmann, B., M. M. Kessels, and R. B. Kelly.** 2000. Molecular links between endocytosis and the actin cytoskeleton. J. Cell Biol. **150:**F111–F116.
50. **Raucher, D., T. Stauffer, W. Chen, K. Shen, S. Guo, Y. J. D., M. P. Sheetz, and T. Meyer.** 2000. Phosphatidylinositol 4,5-bisphosphate functions as a second messenger that regulates cytoskeleton-plasma membrane adhesion. Cell **100:**221–228.
51. **Rizzuto, R., W. Carrington, and R. A. Tuft.** 1998. Digital imaging microscopy of living cells. Trends Cell Biol. **8:**288–292.
52. **Ross, P. E., S. S. Garber, and M. D. Cahalan.** 1994. Membrane chloride conductance and capacitance in Jurkat T lymphocytes during osmotic swelling. Biophys. J. **66:**169–187.
53. **Sandison, D. R., R. M. Williams, K. S. Wells, J. Strickler, and W. W. Webb.** 1995. Quantitative fluorescence confocal laser scanning microscopy (CLSM), p. 39–53. *In* J. B. Pawley (ed.), Handbook of biological confocal microscopy, 2nd ed. Plenum Press, Inc., New York, N.Y.
54. **Sechi, A. S., and J. Wehland.** 2000. The actin cytoskeleton and plasma membrane connection: PtdIns(4,5)P_2 influences cytoskeletal protein activity at the plasma membrane. J. Cell Sci. **113:**3685–3695.
55. **Solsona, C., B. Innocenti, and J. M. Fernandez.** 1998. Regulation of exocytotic fusion by cell inflation. Biophys. J. **74:**1061–1073.
56. **Stauffer, T. P., S. Ahn, and T. Meyer.** 1998. Receptor-induced transient reduction in plasma membrane PtdIns(4,5)P_2 concentration monitored in living cells. Curr. Biol. **8:**343–346.
57. **Streb, H., R. F. Irvine, M. J. Berridge, and I. Schulz.** 1983. Release of Ca^{2+} from a nonmitochondrial intracellular store in pancreatic acinar cells by inositol-1,4,5-trisphosphate. Nature **306:**67–69.
58. **Takenawa, T., and T. Itoh.** 2001. Phosphoinosides, key molecules for regulation of actin cytoskeletal organization and membrane traffic from the plasma membrane. Biochim. Biophys. Acta **1533:**190–206.
59. **Tall, E. G., I. Spector, S. N. Pentyala, I. Bitter, and M. J. Rebecchi.** 2000. Dynamics of phosphatidylinositol 4,5-bisphosphate in actin-rich structures. Curr. Biol. **10:**743–746.
60. **Terebiznik, M. R., O. V. Vieira, S. L. Marcus, A. Slade, C. M. Yip, W. S. Trimble, T. Meyer, B. B. Finlay, and S. Grinstein.** 2002. Elimination of host cell PtdIns(4,5)P_2 by bacterial SigD promotes membrane fission during invasion by Salmonella. Nat. Cell Biol. **4:**766–773.
61. **Thorn, H., K. G. Stenkula, M. Karlsson, U. Ortegren, F. H. Nystrom, J. Gustavsson, and P. Strafors.** 2003. Cell surface orfices of caveolae and localization of caveolin to the necks of caveolae in adipocytes. Mol. Biol. Cell **14:**3967–3976.
62. **Toker, A.** 1998. The synthesis and cellular roles of phosphatidylinositol 4,5-bisphosphate. Curr. Opin. Cell Biol. **10:**254–261.
63. **Toker, A., and L. C. Cantley.** 1997. Signalling through the lipid products of phosphoinositide-3-OH kinase. Nature **387:**673–676.
64. **van der Wal, J., R. Habets, P. Varnai, T. Balla, and K. Jalink.** 2001. Monitoring agonist-induced phospholipase C activation in live cells by fluorescence resonance energy transfer. J. Biol. Chem. **276:**15337–15344.
65. **Vanhaesebroeck, B., S. J. Leevers, K. Ahmadi, J. Timms, R. Katso, P. C. Driscoll, R. Woscholski, P. J. Parker, and M. D. Waterfield.** 2001. Synthesis

and function of 3-phosphorylated inositol lipids. Annu. Rev. Biochem. **70:** 535–602.

66. **van Rheenen, J., and K. Jalink.** 2002. Agonist-induced PIP_2 hydrolysis inhibits cortical actin dynamics: regulation at a global but not at a micrometer scale. Mol. Biol. Cell **13:**3257–3267.
67. **Varnai, P., and T. Balla.** 1998. Visualization of phosphoinositides that bind pleckstrin homology domains: calcium- and agonist-induced dynamic changes and relationship to myo-[^{3}H]inositol-labeled phosphoinositide pools. J. Cell Biol. **143:**501–510.
68. **Watt, S. A., G. Kular, I. N. Fleming, C. P. Downes, and J. M. Lucocq.** 2002. Subcellular localization of phosphatidylinositol 4,5-bisphosphate using the pleckstrin homology domain of phospholipase C delta1. Biochem. J. **363:** 657–666.
69. **Waugh, M. G., D. Lawson, S. K. Tan, and J. J. Hsuan.** 1998. Phosphatidylinositol 4-phosphate synthesis in immunoisolated caveolae-like vesicles and low buoyant density non-caveolar membranes. J. Biol. Chem. **273:**17115–17121.
70. **Waugh, M. G., S. Minogue, J. S. Anderson, M. dos Santos, and J. J. Hsuan.** 2001. Signalling and non-caveolar rafts. Biochem. Soc. Trans. **29:**509–511.
71. **Xu, C., and J. L. Prince.** 1997. Gradient vector flow: a new external force for snakes, p. 66–71. *In* (ed.), IEEE Proceedings of the Conference on Comparisons of Visual Pattern Recognition. IEEE Computer Society Press, Los Alamitos, Calif.
72. **Zampighi, G. A., M. Kreman, K. J. Boorer, D. D. F. Loo, F. Beznilla, G. Chandy, J. E. Hall, and E. M. Wright.** 1995. A method for determining the unitary functional capacity of cloned channels and transporters expressed in Xenopus laevis oocytes. J. Membr. Biol. **148:**65–78.
73. **Zhang, Y., and O. P. Hamill.** 2000. On the discrepancy between whole cell and membrane patch mechanosensitivity of Xenopus oocytes. J. Physiol. (London) **523:**101–115.